Chapter 5

Electron Transfer and Electrocatalytic Studies of Proteins and Protein - Single Walled Carbon Nanotube Composites on Aromatic Self-Assembled Monolayers

In this chapter, we discuss the electron transfer and electrocatalytic properties of proteins on aromatic self-assembled monolayers. Aromatic self-assembled monolayers due to their rich π electron density facilitate better electron transfer compared to the aliphatic self-assembled monolayers. The properties of proteins on surfaces depend on immobilization techniques. Therefore the proteins have been immobilized using different immobilization methods, namely by covalent, non-covalent and by electrochemical potential cycling. The functionalized self-assembled monolayers used were 4-aminothiophenol (4-ATP) and 4-mercaptobenzoic acid (4-MBA). The proteins which we have studied are cytochrome *c* (Cyt *c*), myoglobin (Myb), and horseradish peroxidase (HRP). To enhance the properties of proteins on self-assembled monolayers, the protein-SWNT composites have been formed on SAMs non-covalently by simple adsorption process as well as electrochemically by potential cycling. The protein and protein-SWNT composite modified surfaces were characterized using cyclic voltammetry (CV), electrochemical impedance spectroscopy (EIS), and chronoamperometry (CA). The immobilized surfaces were characterized by atomic force microscopy (AFM) and scanning tunneling microscopy (STM).

5.1 Introduction

Electron transfer reactions play an important role in biological processes. Direct electron transfer of redox proteins on electrode surfaces using surface immobilized protein films is gaining importance as it provides significant insight into the functioning of biological systems and in the development of biosensors. The study of direct electron transfer from protein to electrode surface and their electrocatalytic reactions can serve as models to understand the electrocatalytic reactions and the electron transfer mechanism in biological systems [1]. An understanding of

these reactions fundamentally can provide information on intrinsic redox behavior of proteins and physiological electron transfer processes. In addition, redox proteins are potentially useful for the development of amperometric biosensors and bioelectrocatalytic system.

To study the direct electron transfer, proteins has to be immobilized on the electrode surface. The immobilization of proteins on a bare electrode surface leads to irreproducible behavior. Hence, proteins have to be immobilized on to the modified surfaces. Different types of modification procedures have been reported in the literature. These include covalent attachment, adsorption non-covalent attachment such as electrostatic, hydrophilic, entrapment etc.,

Self–assembled monolayers are molecular assemblies that are spontaneously and chemically adsorbed on a solid surfaces [2]. The self-assembled monolayers formed by the chemisorption of thiols on gold are receiving much attention because of the degree control over the molecular architecture they offer for the facile formation of chemically, and structurally well-defined surfaces. The ability to control surface properties at the nanometer level has important implications in many areas, such as biocompatible materials and biosensors. Immobilizing redox proteins with intact conformations on electrode surfaces is an important task, since many metalloproteins often denature when they adsorb on a solid surface. One way to solve the problem is to immobilize on organic thiol monolayers, surfactants etc., on the electrode surface [3-10].

Ensuring the bioactivity of the immobilized redox protein on the confined environment of a surface is a major challenge in these studies. Recently, there has been significant interest in biological applications of nanomaterials such as metal nanoparticles and carbon nanotubes to change the properties of protein [11-17]. They find potential applications in electroanalysis of redox active biomolecules [11]. It is reported that protein stability is enhanced on the highly curved single walled carbon nanotubes [18]. Moreover, the SWNTs exhibit a highly hydrophobic surface character. The biomolecules can be attached non-covalently through hydrophobic interactions or covalently to carbon nanotubes via linker molecules [19,20]. Prior to their attachment, SWNTs are dispersed in the medium with the aid of polymers or surfactants [21-23].

The amperometric protein biosensors normally rely on the redox current due to hydrogen peroxide reaction, which is a product of enzymatic reaction. However, problem arises due to the high oxidation potential of hydrogen peroxide, which leads to interferences by other oxidizable species such as ascorbic acid, uric acid and acetaminophenol, which are usually present in the

biological samples. On the other hand the reduction of hydrogen peroxide in the presence of a catalyst takes place at much lower potential. The interfering species are electrochemically inactive at this potential and therefore this method is quite attractive for biosensor development. The electron transfer rate and electrocatalytic activity of enzymes strongly depends on immobilization technique and the type of monolayer used for immobilization. One of the most important and well-characterized model systems for immobilization of enzymes is self-assembled monolayers of alkane thiols on gold. Electron transfer mechanism of protein has been studied on self-assembled monolayer of alkane thiols [24,25]. Recently, functionalized aromatic thiols have received much attention for studying electron transfer mechanism of immobilized proteins. Aromatic thiols facilitate better electron transfer because of their π-conjugation. For example, Imabayashi *et al.* [26] immobilized the proteins on aromatic thiol such as 4-mercaptobenzoic acid and showed that they exhibit better electron transfer property compared to the alkanethiols. 4-aminothiophenol (4-ATP) forms a well-organized monolayer showing $\sqrt{3}x\sqrt{3}$ R 30^0 structure on gold [27,28]. Several groups have used SAM of 4-ATP to immobilize the species on the electrode surface covalently [29-32]. The previous attempts to immobilize the protein on the self-assembled monolayer films used carboxyl, pyridine and imidazole terminated alkanethiols [33,34]. Davis *et al.* [35] have used cysteine modified surface for binding of enzyme for surface immobilization.

In this chapter, we describe the effect of immobilization on the electron transfer and electrocatalytic activity of proteins on aromatic self-assembled monolayers of 4-ATP and 4-MBA. To enhance these properties, protein-SWNT composites have been immobilized on the SAMs. The electron transfer and electrocatalytic properties have been studied using CV, EIS, and CA and the immobilized surfaces were studied using scanning probe techniques.

5.2 Experimental Section

5.2.1 Chemicals

We have used the following analytical grade reagents: cytochrome *c* (Fluka), Myoglobin (Sigma), Horseradish peroxidase (Sigma), 4-aminothiophenol (Aldrich), 4-mercaptobenzoic acid (Aldrich), 1-Ethyl-3-(3-dimethylaminopropyl)-carbodiimide (EDC) (Aldrich), sodium phosphate dibasic Na_2HPO_4 (Rankem), sodium dihydrogen phosphate (Merck), hydrogen peroxide (H_2O_2)

solution 30% (Merck). All the solutions were prepared using Milli-Q water of resistance 18 MΩ cm. protein solution was made by dissolving 2 mg of protein in 0.3 ml of phosphate buffer solution of pH 6.5.

5.2.2 Purification of Single Walled Carbon Nanotubes (SWNTs)

The single walled carbon nanotube obtained from Carbolex Co. USA has been purified as reported earlier [36]. In brief, the raw soot SWNT was subjected to air oxidation by heating the sample in air at 350 ^{0}C for 4 hours to oxidize the non-tubular form of the carbon. The SWNT material was then refluxed with 6N nitric acid for 30 min in order to dissolve the metal particles. After cooling, the sample was filtered using a cellulose nitrate filter paper with 0.2 μm pore size by applying vacuum suction. A clear green colored supernatant acidic solution was collected at the bottom of filtering unit. Successive washing with Milli-Q water removes the substantial amount of trapped acid form the sediment. The SWNTs collected in the filter paper was dried in an air oven at 50 ^{0}C for 30 min.

5.2.3 Electrode Pretreatment

All electrochemical experiments were carried out using gold disc of geometric area 0.002 cm^2 as a working electrode. Immediately before use, the poly crystalline gold disc electrode was polished with emery paper of grade 800 and 1500, followed by polishing in aqueous slurries of 1 μm, 0.3 μm and finally with 0.05 μm alumina slurries, ultrasonicated in water to remove alumina particles for 1 minute and then cleaned with dil. aquaregia (3:1:4 mixture of conc. HCl, conc. HNO_3 and water) for one minute before each experiment. Finally, it was rinsed in distilled water thoroughly, followed by rinsing in Milli-Q water and ethanol before SAM formation. The true surface area of the disc electrode was measured by potential cycling in 0.1M $HClO_4$.

5.2.4 Self-Assembled Monolayer Formation

The self-assembled monolayer of 4-Aminothiophenol (4-ATP) or 4-mercaptobenzoic acid (4-MBA) was formed by placing the cleaned gold disc electrode in 1 mM ethanol solution of 4-ATP or 4-MBA for 12 hours. The electrode was taken out from the thiol solution, rinsed with ethanol and finally with milli-Q water.

5.2.5 Proteins Immobilization on 4-ATP and 4-MBA

Covalent immobilization of proteins were carried out by immersing 4-ATP modified Au electrode in a 30% glutaraldehyde for 24 hours. The electrode was taken out from gluaraldehyde, rinsed with water and placed in protein solution at 4 ^{0}C and pH 6.5 for 24 hours. The electrode was taken out from the protein solution, washed with phosphate buffer solution for several times, followed by Milli-Q water to remove any non-specific bound protein on the surface.

Proteins were covalently attached to the surface by immersing 4-MBA modified Au electrode in EDC solution. The electrode was taken out from EDC, rinsed with water and placed in protein solution at 4 ^{0}C of pH 6.5 for 24 hours. The electrode was then taken out from the protein solution, washed with phosphate buffer solution for several times, followed by Milli-Q water to remove any non-specific bound enzyme on the surface.

Non-covalent adsorption was carried out at 4 ^{0}C onto the 4-ATP or 4-MBA self-assembled monolayer modified gold surface by immersing in a 2 mg of protein in a 0.3 ml of 0.1M sodium phosphate buffer solution of pH 6.5. The electrode was taken out from the protein solution, washed with phosphate buffer followed by rinsing in Milli-Q water.

Proteins were immobilized at room temperature onto the 4-ATP or 4-MBA self-assembled monolayer modified gold surface by potential cycling in a microcell containing protein solution. The electrode was taken from protein solution, washed with phosphate buffer solution followed by rinsing in Milli-Q water.

5.2.6 Immobilization of Protein-SWNT on Monolayer Modified Surface

5.2.6.1 Dispersion of SWNT in Protein Solution

Homogeneous and well-dispersed CNTs in aqueous and non-aqueous media were reported earlier with the aid of polymers and surfactants [21-23,37-39]. Here we have used analogous method to disperse the SWNTs in phosphate buffer solution. 2 mg of protein was dissolved in 0.3 ml of 0.1M phosphate buffer solution of pH 6.5. Dispersion of NTs in protein solution has been reported recently by sonication under ice cold water [40,41]. In the present work, we have followed similar procedure to disperse SWNTs. In brief, purified SWNTs were added into the protein solution and sonicated. The protein helps in better solubilization of SWNTs in phosphate buffer.

The 4-ATP or 4-MBA modified gold disc electrode was placed in the freshly prepared dispersion of protein-SWNT for 24 hours at 4 ^{0}C. The electrode was taken out and washed with phosphate buffer solution followed by Milli-Q water. During the formation of the dispersion by sonication under ice cold water, the protein in the solution functionalizes the SWNTs by hydrophobic interaction.

Protein-SWNT was immobilized at room temperature onto the 4-ATP or 4-MBA self-assembled monolayer modified gold surface by potential cycling in a microcell containing protein-SWNT dispersion solution. The electrode was taken from protein-SWNT solution, washed with phosphate buffer solution followed by rinsing in Milli-Q water. Table 1 gives the different proteins and protein-SWNT composites immobilized on 4-ATP and 4-MBA surface and schematic of the covalent immobilization is shown in Figure 1 and Figure 2.

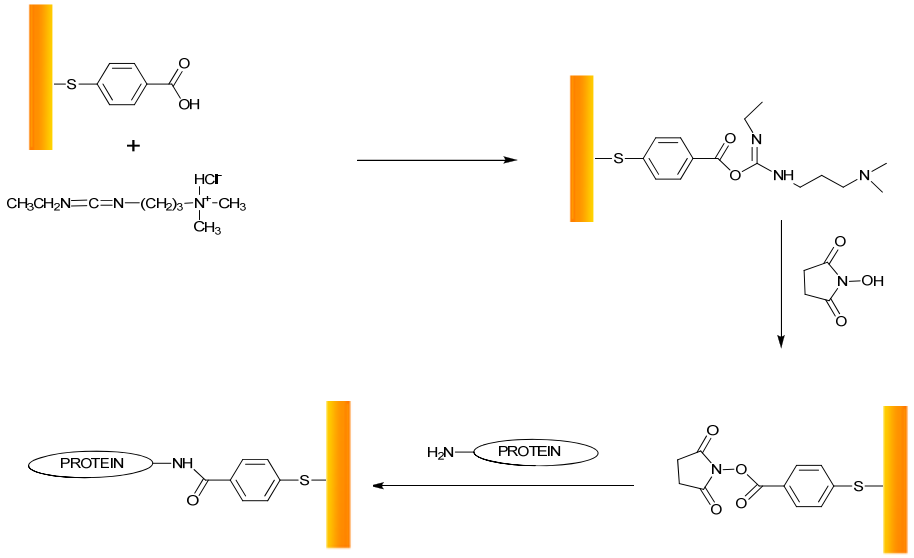

Figure 1. Schematic of the covalent attachment of the protein to the carboxyl terminated surfaces.

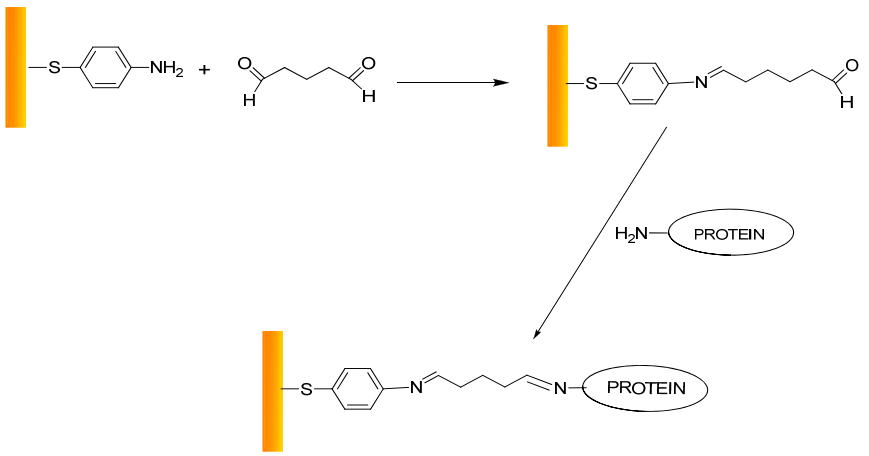

Figure 2. Schematic representation of the covalent modification of proteins to the amine terminated surfaces.

Methods of Immobilization	Protein		
	Cytochrome *c* (Cyt *c*)	Myoglobin (Myb)	Horseradish peroxidase (HRP)
Covalent	Cyt *c*/GA/4-ATP/Au Cyt *c*/EDC/4-ATP/Au	Myb/GA/4-ATP/Au Myb/EDC/4-MBA/Au	HRP/GA/4-ATP/Au HRP/EDC/4-ATP/Au
Non-covalent	Cyt *c*/4-ATP/Au Cyt *c*/4-MBA/Au	Myb/4-ATP/Au Myb/4-MBA/Au	HRP/4-ATP/Au HRP/4-MBA/Au
Electrochemical	ECyt *c*/4-ATP/Au ECyt *c*/4-MBA/Au	EMyb/4-ATP/Au EMyb/4-MBA/Au	EHRP/4-ATP/Au EHRP/4-MBA/Au
Non-Covalent (protein-SWNT)	Cyt *c*-SWNT/4-ATP/Au Cyt *c*-SWNT/4-MBA/Au	Myb-SWNT/4-ATP/Au Myb-SWNT/4-MBA/Au	HRP-SWNT/4-ATP/Au HRP-SWNT/4-MBA/Au
Electrochemical (protein-SWNT)	ECyt *c*-SWNT/4-ATP/Au ECyt *c*-SWNT/4-MBA/Au	EMyb-SWNT/4-ATP/Au EMyb-SWNT/4-MBA/Au	EHRP-SWNT/4-ATP/Au EHRP-SWNT/4-MBA/Au

Table 1. Different methods used to immobilize proteins and protein-SWNT composites on 4-ATP and 4-MBA surface. (Cytochrome *c* = Cyt *c*, Myoglobin = Myb, Horseradish peroxidase = HRP, 4-ATP = 4-Aminothiophenol, 4-MBA = 4-Mercaptobenzoic acid, GA = glutaraldehyde, EDC = 1-Ethyl-3-(3-dimethylaminopropyl)-carbodiimide).

5.2.7 Evaporated Gold Surface

Evaporated gold (~100nm thickness) on glass with chromium under layers (2-5 nM thickness) was used. The substrate was heated to 350 ^{0}C during gold evaporation under a vacuum pressure of 2x10^{-5} m bar, a process that normally yields predominantly Au (111) orientation.

Evaporated gold surface was cleaned in a piranha solution (a mixture of 30% H_2O_2 and concentrated H_2SO_4 in a 1:3 ratio) before use. (*Caution! Piranha solution is very corrosive.*)

5.2.8 AFM and STM studies

All AFM and STM studies were carried out using evaporated gold specimen. The images were taken using Pico plus (Molecular Imaging) instrument in ac mode (Tapping mode) at a frequency 175 kHz with a cantilever of silicon of type PPP-NCL-50 from nanosensors, USA. All the STM images were obtained at ambient temperature in air in constant current mode. An electrochemically etched tungsten tip was used as the probe. The images shown here were plane corrected using scanning probe image processor (SPIP) software (Image metrology, Denmark). To ensure that the images shown here are representative of the surface, multiple images were obtained at different locations and scan ranges. All the studies have been carried out with the specimens obtained from the same sample plate.

5.3 Results and Discussions

5.3.1 Studies of Covalent (Cyt c/GA/4-ATP/Au) and Non-covalent (Cyt *c*/4-ATP/Au) Immobilization of Cyt *c* on Aromatic Self-Assembled Monolayers of 4-ATP

The molecular weight of Cyt *c* is 12, 400 which consists of a single polypeptide chain of 104 amino acid residues and covalently attached to a heme group [42-43]. Cyt *c* has 19 positively charged lysine residues, two arginines which are also positively charged, and 12 acidic residues (aspartic or glutamic acids). Cyt *c* is very basic with an isoelectric point near pH 10. Isoelectric point is the pH at which the number of positive charges and the number of negative charges of a compound are equal. The active site in Cyt *c* is Fe (II). Cyt *c* is a water soluble heme protein that lies in the inner membrane of the mitochondria. Cyt *c* is a ideal model protein, as its three-dimensional structure has been well characterized. Since it is redox protein and with heme iron undergoing redox reaction, its electrochemistry is widely studied and quite well understood. Cyt *c* has been widely used to study their electron transfer (ET) rate and electro catalytic activity. This heme protein offers the particular advantage that it can be immobilized on electrodes in a well-defined manner using different strategies.

5.3.1.1 Atomic Force Microscopy (AFM) Studies

Figure 3a is the tapping mode AFM image of self-assembled monolayer of 4-ATP on evaporated gold surface and the Figure 3b, that of Cyt *c* adsorbed non-covalently on the surface by hydrophilic interaction with the self-assembled monolayer of 4-ATP on gold. The protein is distributed densely in several regions forming few large clusters in addition to smaller aggregates in several regions. The large clumps have a height of 100 –150 nm and 1 - 2 µm cross section.

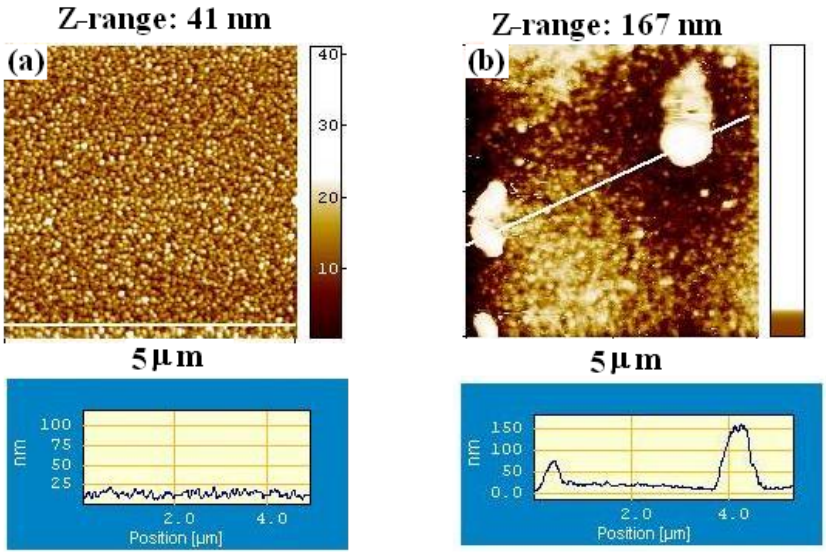

Figure 3. AFM images of (a) 4-ATP/Au and (b) Cyt *c*/4-ATP/Au surfaces.

5.3.1.2 Scanning Tunneling Microscopy (STM) Studies

We have carried out STM studies on the surface of 4-ATP on gold immobilized with Cyt *c*. Figure 4a is the 500 nm x 500 nm STM image of the surface on which Cyt *c* is immobilized. STM resolves individual protein molecules. The image in Figure 4b shows very clearly resolved individual protein molecules adsorbed on the 4-ATP modified gold surface. The measured sizes of the individual protein molecules are dependent on factors such as orientation of the molecules, tip perspective *vis-a-vis* the surface etc., However, the average size of Cyt *c* molecules measured with this and other several images is about 4-6 nm which is in good agreement with the values reported in literature [10]. The features as observed by STM in several regions indicate that the protein molecules are adsorbed on the entire surface.

Figure 4c shows the STM image of the Cyt *c* immobilized covalently on 4-ATP. Though the image is not quite clear, individual protein molecules of sizes ranging from 4-6 nm can be

seen. It can be clearly seen from the STM images of the non-covalent and covalent immobilization, protein content in the case of non-covalently immobilized Cyt *c* is higher compared to the covalently immobilized Cyt *c*.

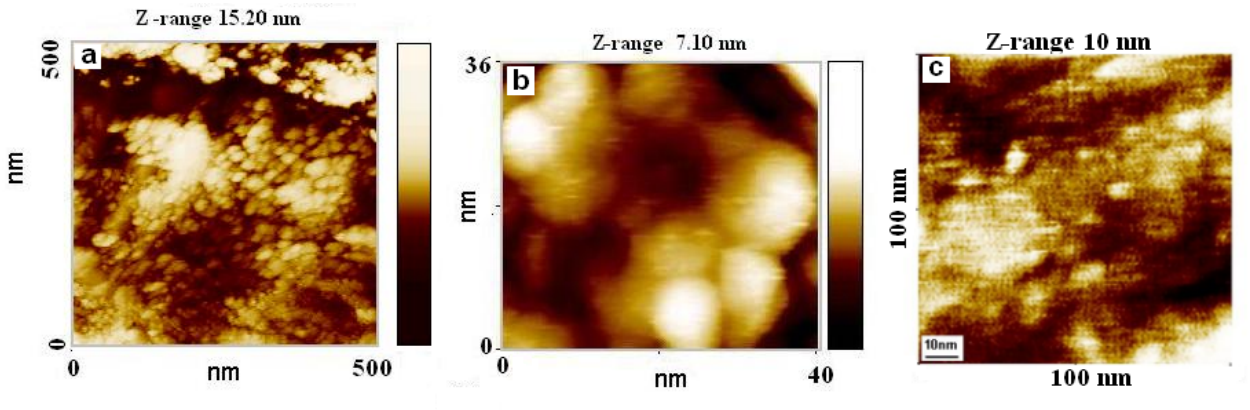

Figure 4. a) STM image of Cyt *c*/4-ATP/Au, b) zoomed portion of (a), the surface showing individual protein clusters, and (c) Cyt *c*/GA/4-ATP/Au.

5.3.1.3 Redox Properties and Surface Concentrations

Figure 5 and 6 shows the cyclic voltammogram of non-covalent (Cyt *c*/4-ATP/Au) and covalent (Cyt *c*/GA/4-ATP/Au) immobilized Cyt *c* on 4-ATP modified gold surface in a phosphate buffer solution of pH 6.5 at different scan rates. The cyclic voltammograms though not well defined show quasi-reversible redox peaks. The broad hump instead of clearly defined peaks shows that the protein molecules and consequently thereby heme moiety are oriented randomly on the surface. This will create a broader energy distribution for the redox process and the potential range through which it occurs is therefore rather ill defined. The half peak potential, which is the average of the cathodic and anodic peak potentials occurs at E^{o1} = 25 mV and 82 mV for non-covalent and covalent immobilized electrodes respectively**.** The half peak potential is characteristic redox potentials of Fe^{2+}/Fe^{3+} couple of immobilized Cyt *c*. As the scan rate (ν) increases the redox peak currents (i_p) of immobilized Cyt *c* increases linearly with scan rate as shown in the inset of Figure 5 and Figure 6 following the expression $i_p = n^2F^2\nu A\Gamma/4RT$, where n=number of electrons, F=Faraday constant, Γ=the number of redox active sites on the surface, A=area, ν=scan rate. This indicates diffusion less surface confined electron transfer processes.

The surface concentrations were calculated from the charge associated with cathodic peak at a scan rate of 50 mV/s of the cyclic voltammetry. The surface concentrations were found

to be 8.6 x 10^{-11} mol cm^{-2} and 2.2 x 10^{-11} mol cm^{-2} after correcting for the roughness factor of 6.8 for the disc electrode of geometric area 0.002 cm^2 for non-covalent and covalent immobilized electrodes. The surface concentration of non-covalent immobilized Cyt c surfaces being higher which is due to multilayer adsorption essentially arising out of hydrophilic interaction. This is also confirmed by the AFM images showing high surface features as will be discussed later in this chapter.

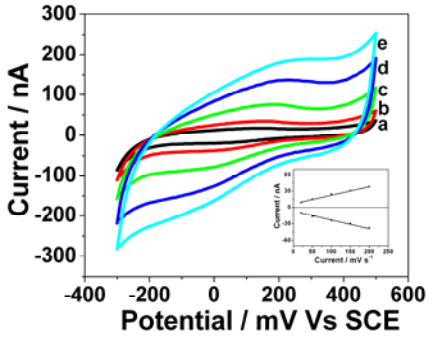

Figure 5. Cyclic voltammograms of Cyt *c*/GA/4-ATP/Au in 0.1M phosphate buffer solution of pH 6.5 at scan rate (mV s^{-1}) of (a) 20, (b) 50, (c) 100, (d) 150, and (e) 200. Inset shows peak current vs scan rate.

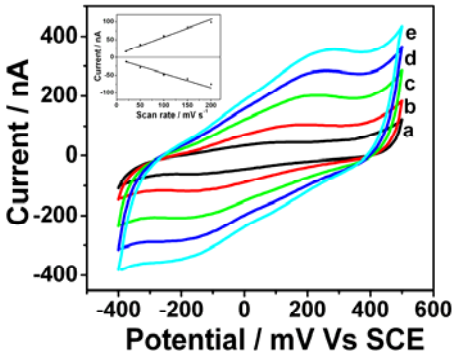

Figure 6. Cyclic voltammograms of Cyt *c*/4-ATP/Au in 0.1M phosphate buffer solution of pH 6.5 at scan rate (mV s^{-1}) of (a) 20, (b) 50, (c) 100, (d) 150, and (e) 200. Inset shows peak current vs scan rate.

5.3.1.4 Electrochemical Impedance Spectroscopy Studies

The impedance spectroscopy of immobilized Cyt *c* electrode was carried out in a phosphate buffer solution. Figure 7a–b shows the impedance plots (Nyquist plots) of the covalent and non-covalent immobilized Cyt *c* on 4-ATP. Insets of Figure 7a–b represent equivalent circuits for the

electroactive monolayers that exhibit electron transfer kinetic limitation. This is a model similar to the equivalent circuit proposed by Nahir and Bowden [7] comprising of a parallel combination of a constant phase element (CPE) represented by Q, charge transfer resistance R_{ct}, adsorption pseudo capacitance C_a in series with the uncompensated solution resistance R_u. The pseudo capacitance arises due to the highly charged state of proteins adsorbed on the electrode surface. We have used the CPE which represents the deviation from the ideal capacitive component instead of the double layer capacitance (C_{dl}) since it provided a much better fit. From the best fit parameters for the impedance plots, the R_{ct} and C_a values obtained for the non-covalently immobilized Cyt *c* were calculated to be 4.12 x 10^6 Ω cm^2 and 6.23 μF cm^{-2} respectively. From these parameters, the electron transfer rate constant was calculated using the formula $k^o_{et} = (2R_{ct}C_a)^{-1}$ [7]. For the non-covalently immobilized Cyt *c* the rate constant value was measured to be 0.01 s^{-1}. This can be compared with the reported value of rate constants 10^{-4}-10^{-1} s^{-1} for Cyt *c* on different self-assembled monolayers adsorbed on gold surface [8]. It is much lower than 0.78 s^{-1} on NaY zeolite particles [45], 0.4 s^{-1} for Cyt *c* immobilized on macro and micro sized carbon electrode [9] and 0.14 s^{-1} reported for Cyt *c* on self-assembled monolayers [25]. The lower electron transfer kinetics may be attributed to the inhomogeneous distribution of Cyt *c* restricting the electron transfer pathway in protein molecule. The R_{ct} and C_a values for the covalently immobilized Cyt *c* are 1.17 x 10^6 Ω cm^2 and 0.72 μF cm^{-2} respectively. The electron transfer rate constant for covalently functionalized Cyt *c* is 0.6 s^{-1}. The rate constant is higher compared to that of the non-covalently immobilized Cyt *c* which is 0.01 s^{-1}. The high electron transfer rate of covalently functionalized Cyt *c* electrode is due to the through bond tunneling mechanism where the electrons from the adsorbed protein flow through the bonds of 4-ATP to the gold surface.

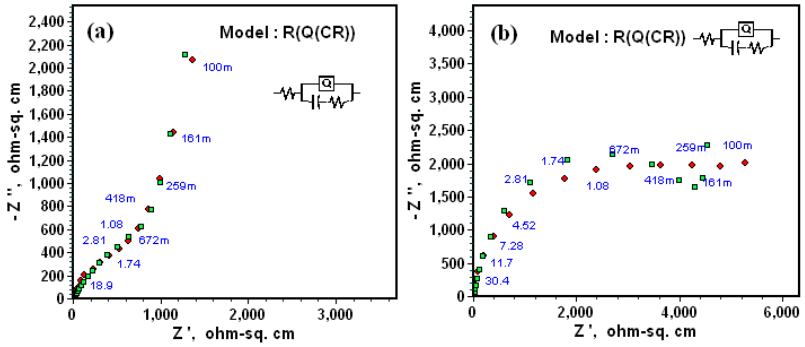

Figure 7. Equivalent circuit fitted impedance plots for a) Cyt *c*/GA/4-ATP/Au and b) Cyt *c*/4-ATP/Au in phosphate buffer solution.

5.3.1.5 Electrocatalysis of Cyt *c* Electrodes to the Reduction of H_2O_2

5.3.1.5.1 Cyclic Voltammetry Studies

Cyt *c* is a heme protein and shows electrochemical response to the reduction of H_2O_2. Electocatalytic activity of Cyt *c* modified electrodes has been studied towards H_2O_2 reduction using cyclic voltammetry. Figure 8 and Figure 9 show the cyclic voltammograms of non-covalent and covalent immobilized Cyt *c* on 4-ATP with successive addition of hydrogen peroxide to phosphate buffer solution of pH 6.5 under N_2 atmosphere. Concentration of H_2O_2 was increased in steps of 3.8 mM. With increasing H_2O_2 concentration, reduction current increases. It can be seen that H_2O_2 reduction current is higher for the non-covalent Cyt *c* electrodes compared to the covalent immobilized Cyt *c* electrodes. The higher reduction current of non-covalent adsorbed Cyt *c* electrodes may be due to the higher concentration of protein on the surfaces as evidenced by the cyclic voltammetry and STM, studies as discussed earlier.

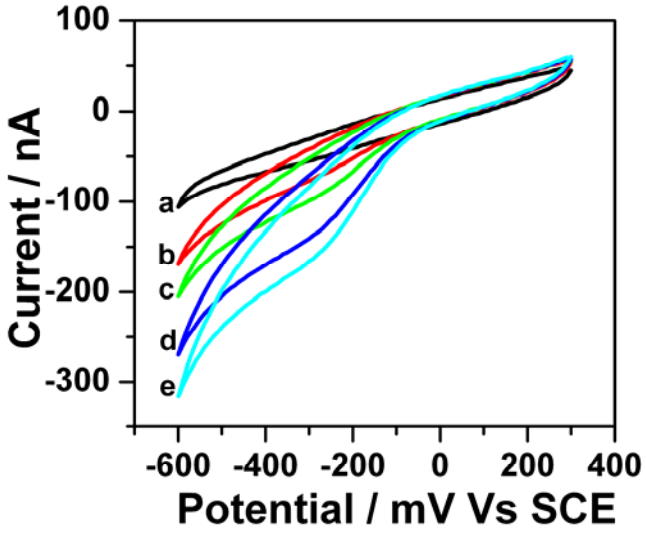

Figure 8. Cyclic voltammograms of Cyt *c*/GA/4-ATP/Au corresponding to the reduction of different concentrations of H_2O_2 in phosphate buffer solution of pH 6.5 at a scan rate of 50 mVs^{-1} under N_2 atmosphere. H_2O_2 concentration was a) 0 mM, b) 3.8 mM, c) 7.6 mM, d) 11.4 mM, and e) 15.2 mM.

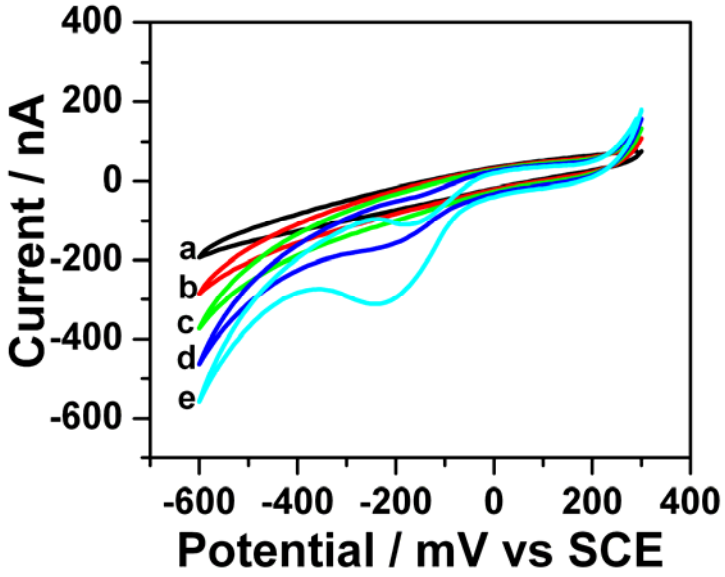

Figure 9. Cyclic voltammograms of Cyt *c*/4-ATP/Au corresponding to the reduction of different concentrations of H_2O_2 in phosphate buffer solution of pH 6.5 at a scan rate of 50 mVs^{-1} under N_2 atmosphere. H_2O_2 concentration was a) 0mM, b) 3.8mM, c) 7.6mM, d) 11.4mM, and e) 15.2mM.

5.3.1.5.2 Chronoamperometric Measurements

The electrocatalytic activity of Cyt *c* electrodes has been characterized towards reduction of H_2O_2 was studied using chronoamperometry. They have been conducted at ambient, stirred conditions in phosphate buffer solution of pH 6.5. Figure 10 is the amperometric responses of 4-ATP and Cyt *c* modified 4-ATP electrodes with successive addition of H_2O_2. Upon addition of an aliquot of H_2O_2 to the buffer solution, the reduction current increases steeply to reach a steady state value within 5 s. The concentration of H_2O_2 was increased in steps of 3.8 mM. The current due to H_2O_2 reduction was considerably higher in the case of non-covalent immobilized electrodes compared to the covalent immobilized electrodes. Linear calibration plots obtained for the electrodes in the concentration range from 3.8 mM to 34.2 mM are shown in the inset of Figure 10. The higher electrocatalytic activity of non-covalently immobilized Cyt *c* when compared to the covalently immobilized Cyt *c* is attributed to the higher surface concentration of protein in the former case. Detection limits for H_2O_2 were determined by adding very small amounts of H_2O_2 until there is a detectable (few nA) change in current. The steady state current

observed was about 4 times the background noise. The detection limits were found to be 800 μM and 400 μM, for the covalent and non-covalent modified electrodes, respectively.

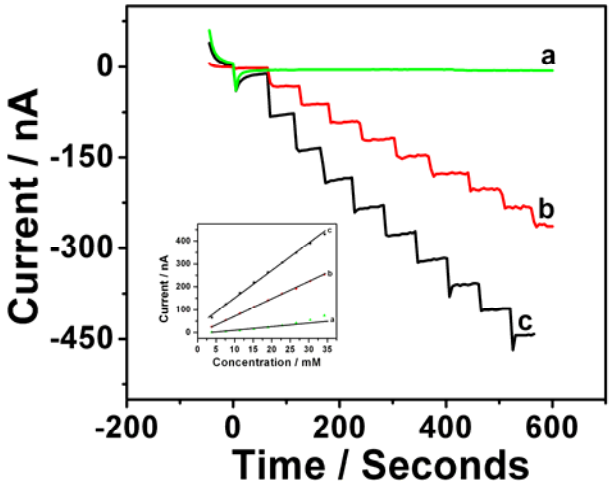

Figure 10. Amperometric response to H_2O_2 with successive addition of 3.8 mM H_2O_2 under stirred conditions in a phosphate solution of pH 6.5 under N_2 atmosphere. a) 4-ATP/Au, b) Cyt *c*/GA/4-ATP/Au and c) Cyt *c*/4-ATP/Au. Applied potential = –110 mV. Inset shows the calibration plots.

5.3.2 Electron Transfer and Electrocatalytic Properties of Cyt *c*-SWNT Immobilized on 4-ATP (Cyt *c*-SWNT/4-ATP/Au)

Since their discovery in 1991 [46], the carbon nanotubes have evoked tremendous interest due to their several unique physical, chemical, mechanical and electrical properties. The single-walled carbon nanotubes (SWNTs) are being studied as a model one-dimensional nanostructures with several unique properties that may be useful in energy conversion devices, molecular electronics and sensor applications. Due to the nanometer size and tunable hydrophobic and hydrophilic properties by functionalization, several biomolecules have the tendency to undergo non-covalent adsorption on carbon nanotubes. Their reported ability to promote electron transfer of several redox proteins can find applications as biosensors.

Several groups have studied the electron transfer properties and electrocatalysis of enzymes, DNA and proteins on CNTs [47-57]. There are also a few reports about the covalent functionalization of enzymes on carbon nanotubes and study of their electron transfer properties [58-60]. Encapsulation and immobilization of phospholipids and proteins has been a subject of

intense interest in recent times with particular emphasis on its ability as intracellular transporter [61-63]. The electrochemical studies on the functionalization of carbon nanotubes (CNT) and attachment of biomolecules suggest that they have the potential to facilitate direct electron transfer by acting as molecular-scale electrical conduits, and for designing nanoscale biosensors [64-67].

Here, we used a method of combining the affinity of the redox proteins to SWNT surface and its non-covalent binding to the 4-ATP SAM on gold. Using cyclic voltammetry, we have studied the surface concentrations, electron transfer properties and electrocatalysis on the SAM of 4-ATP. Electrochemical impedance studies have been used to calculate the rate constants. The Cyt *c*-SWNT modified surfaces were characterized by atomic force microscopy and scanning tunneling microscopy.

5.3.2.1 AFM and STM Studies

Figure 11a is the tapping mode AFM image of the surface adsorbed with the protein and the SWNTs. Figure 11b is the zoomed portion of the image 9a. There are several regions where the clusters of proteins on the surface can be seen. These clusters are of varying sizes and are scattered on the surface. Interestingly, there are some long rods like features, which are seen in the image. These are found to be distributed throughout different regions of the image scanned. These features correspond to the Cyt *c* covered SWNTs. Cyt *c* wraps around the SWNTs, since the hydrophobic core of the Cyt *c* covers the surface of SWNT by hydrophobic interaction, while the outer surface of protein, which is hydrophilic binds strongly to the amino groups of the 4-ATP on gold by hydrophilic interaction through hydrogen bonding. Figure 12 shows the single rod like features of the Cyt *c*-SWNT. The width of the rod like features vary from 100–150 nm and the height features from 10 –12 nm. This observation rules out the possibility of line features being bundles of CNTs. Curiously the length of the line features in some regions are larger than 3 μm and varying from 500 nm –1 μm. Since the acid treated CNTs are only 100 nm –150 nm in length, the long rods obviously do not correspond to the long axis of the SWNTs. This suggests the possibility that these features may correspond to the parallel arrangement of SWNTs along with the protein.

To confirm the above finding and to obtain the finer features, we have conducted STM studies on the surface of 4-ATP on gold immobilized with Cyt *c* adsorbed SWNT. Figure 13

shows the STM scan on the surface immobilized with the Cyt *c* covered SWNT. Several sharp striations and steps which arrange themselves in layers are clearly seen. Figure 13b shows the zoomed portion of the image in Figure 13a. This portion of the image clearly resolves the individual carbon nanotubes covered with Cyt *c* molecules. The width of the individual striation is about 5–6 nm corresponding to an average size of the protein molecules confined on SWNT. These well aligned Cyt *c* functionalized CNTs are present in all the regions of the image in Figure 13a and also in several other regions scanned as shown in the Figure 14a-d. The protein clusters shown in Figure 13 and 14 are actually Cyt *c* covered SWNTs acting as a bunch of molecular wires. We would like to point out here that such well aligned enzyme covered SWNTs have not been previously reported in literature.

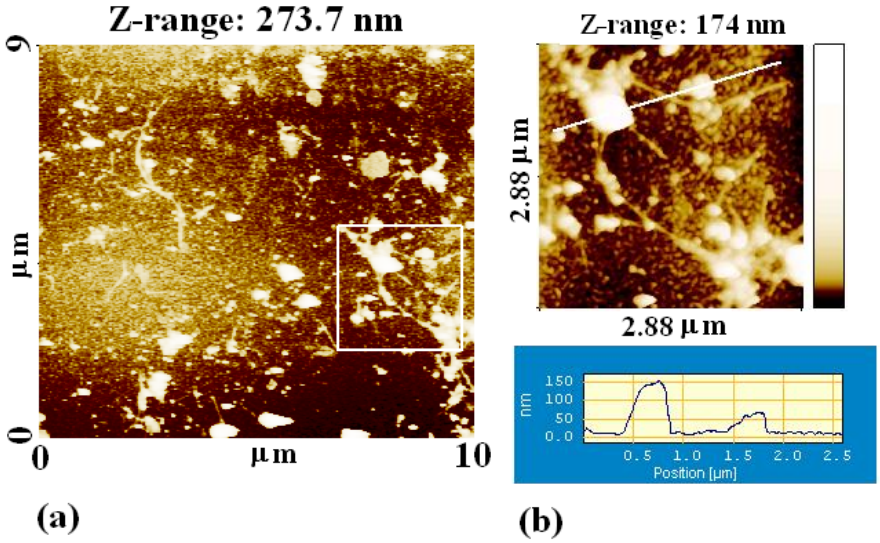

Figure 11. AFM images of (a) Cyt *c*/SWNT/4-ATP/Au and (b) Zoomed portion of 9a and corresponding line scan is shown below the image.

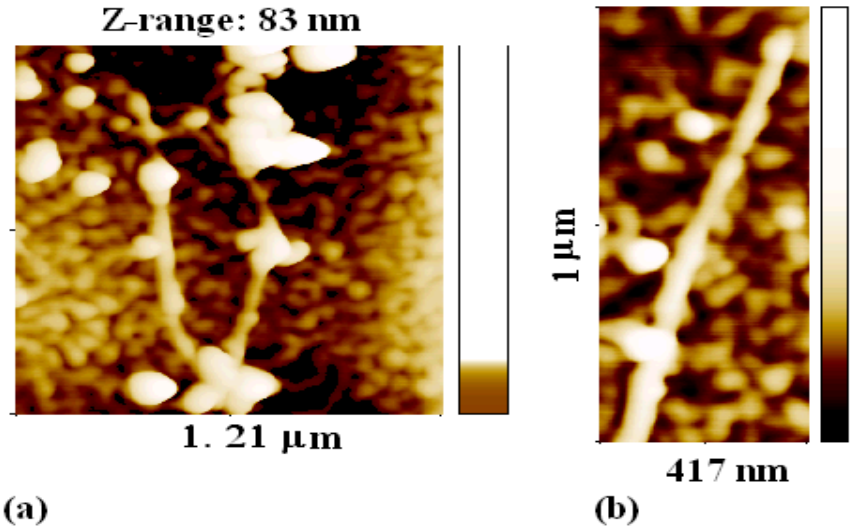

Figure 12. (a-b) AFM images of Cyt *c*/SWNT/4-ATP/Au.

It is known that the Cyt *c* is positively charged due to the cationic lysine residues being exposed at the outer region of the protein. This is the basis for the extensive studies being carried out on the adsorption of protein by electrostatic interaction on the negatively charged carboxyl terminated alkanethiols [6]. This approach has been quite successful in immobilizing the redox protein on the negatively charged surfaces and for the study of the electron transfer properties. However, the horse Cyt *c* has large dipole moment of about 300 D due to asymmetric distribution of 15 negatively charged residues consisting of glutamic and aspartic acids and more homogeneous distribution of 21 positively charged lysine and arginine residues. The driving force for the organization of the Cyt *c* functionalized SWNTs in the present case is due to the negative charges which may provide the necessary attractive electrostatic binding sites for the redox protein. This leads to an attractive electrostatic interaction between the positively charged amino groups of 4-ATP and the negatively charged Cyt *c* covered CNTs. In addition, there is a hydrophilic interaction between protein with carboxylic groups of proteins and the amino groups of the 4-ATP. The enzyme immobilization is therefore brought about by a combination of hydrophilic, electrostatic and van der Waals interactions among the protein molecules, 4-ATP and SWNTs. The regular alignment of CNTs can be due to the interaction of the Cyt *c* with 4-ATP and the neighboring protein-SWNTs. The protein molecules adsorbed on SWNTs are well ordered and the molecular interactions between neighboring protein units of different SWNTs bring about the required lateral association of the functionalized SWNTs.

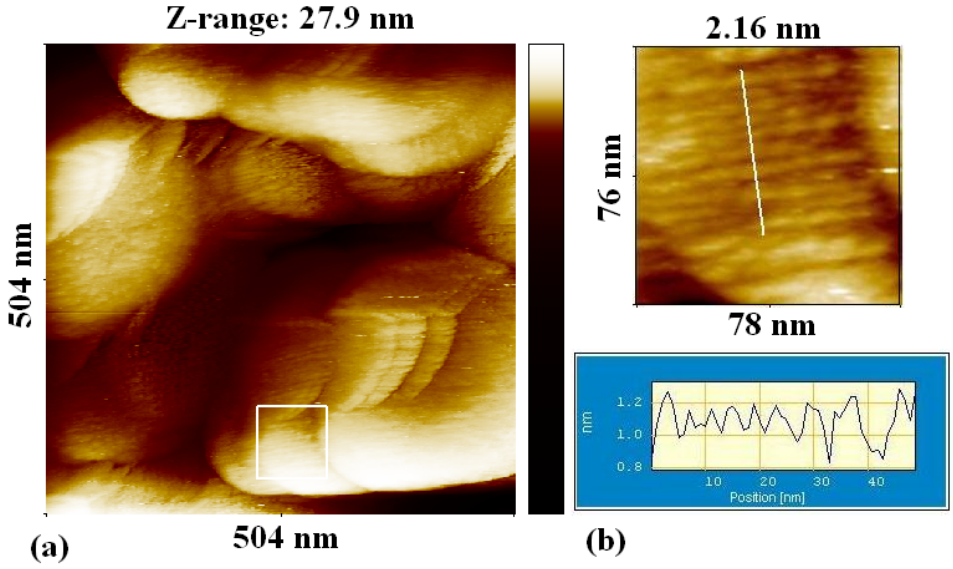

Figure 13. STM image of (a) Cyt *c*/SWNT/4-ATP/Au (b) Zoomed Portion of 11a.

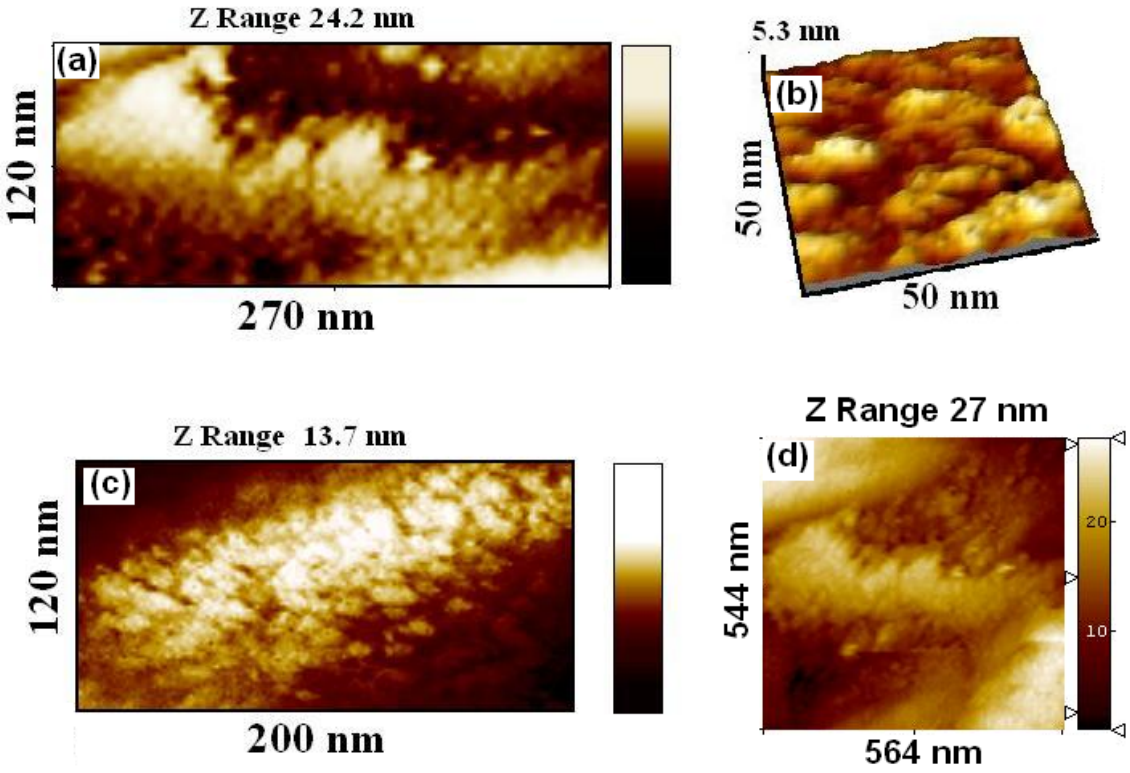

Figure 14. STM images of the different regions of the Cyt *c*/SWNT/4-ATP/Au surface showing the aligned Cyt *c* covered SWNTs.

5.3.2.2 Redox Properties

Cyclic voltammetry (CV) has been used for electrochemical characterization of the Cyt *c*-SWNT on SAM of 4-ATP as they provide significant insight into the surface concentration of the protein, electron transfer process and electrocatalysis. From the integration of the reduction peak of Cyt *c* at a scan rate of 50 mVs^{-1}, the surface coverage was calculated.

Figure 15 shows the cyclic voltammograms of Cyt *c*-SWNT on SAM of 4-ATP in phosphate buffer solution of pH 6.5. The redox peak current increases linearly with the scan rate as shown in the inset of Figure 15. The peak current is related to the scan rate by $i_p = n^2F^2\nu A\Gamma/4RT$, where n=number of electrons, F=Faraday constant, Γ=the number of redox active sites on the surface, A=area, ν=scan rate, indicating a typical of diffusionless surface confined processes. The half peak potential (E^{01}) calculated by averaging the cathodic and anodic potentials was found to be 11.25 mV verses SCE.

The surface coverage of Cyt *c* functionalized SWNTs on SAM of 4-ATP is measured to be about 6.3 x 10^{-11} mol cm^{-2}. This value is larger than the value of monolayer concentration of Cyt *c*. High surface concentrations are due to the multilayer adsorption of protein [12]. The multilayer adsorption of protein on 4-ATP monolayer have been confirmed in the AFM and STM images which show large 'Z' values corresponding to surface heights.

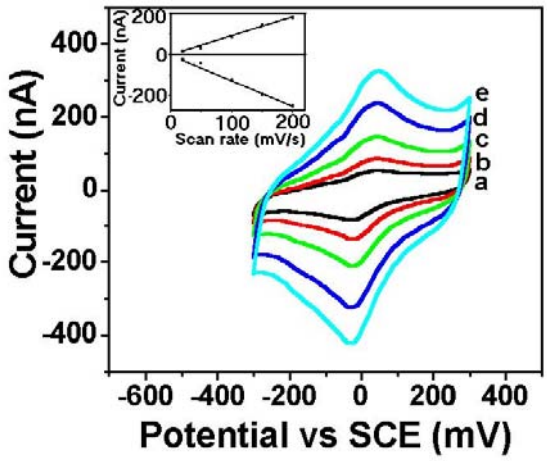

Figure 15. Cyclic voltammograms of Cyt *c*/SWNT/4-ATP/Au electrode in 0.1M Phosphate buffer solution of pH 6.5 under N_2 atmosphere at scan rates (mVs^{-1}) of (a) 20, (b) 50, (c) 100, (d) 150, and (e) 200. Inset shows the plot of peak current vs. scan rate.

5.3.2.3 Electrochemical Impedance Spectroscopy (EIS) Studies

The impedance spectroscopy of immobilized Cyt *c*-SWNT electrode was carried out in a phosphate buffer solution. Figure 16 shows the impedance plots (Nyquist plots) of the Cyt *c*-SWNT on 4-ATP. Insets of Figure 16 represent equivalent circuits for the electroactive monolayers that exhibit electron transfer kinetic limitation. This is a model similar to the equivalent circuit proposed by Nahir and Bowden [7] comprising of a parallel combination of a constant phase element (CPE) represented by Q, charge transfer resistance R_{ct}, adsorption pseudo capacitance C_a in series with the uncompensated solution resistance R_u. The pseudo capacitance arises due to the highly charged state of proteins adsorbed on the electrode surface. We have used the CPE which represents the deviation from the ideal capacitive component instead of the double layer capacitance (C_{dl}) since it provided a much better fit. The electron transfer rate constant of Cyt *c* functionalized SWNT on 4-ATP is 2.9 s^{-1}. This value is higher than that of the Cyt *c* without SWNTs on 4-ATP surface. It has been reported previously that the lateral interactions among adjacent adsorbed proteins contribute to protein deactivation in harsh environments. The large increase in electron transfer rate constant of Cyt *c* while being covered around carbon nanotubes can be explained due to two factors. The suppression of the neighboring protein–protein interaction on SWNTs can free the individual protein molecules thereby facilitating easy electron transfer reaction from and to the electrode surface [18]. Again, the rate of electron transfer can increase if the Cyt *c* functionalized SWNTs connect the redox active site of proteins by acting as nanoscale wires.

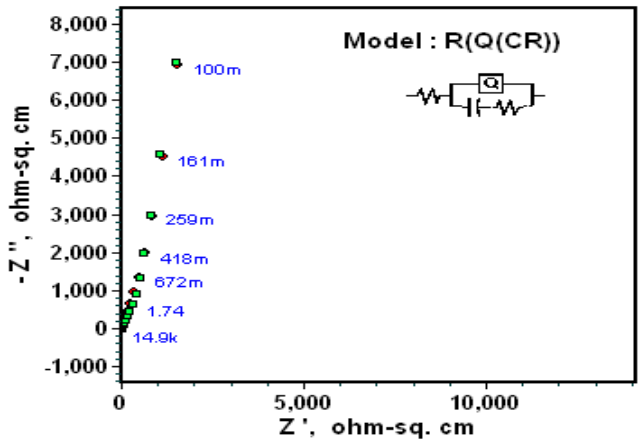

Figure 16. Equivalent circuit fitted impedance plots for Cyt *c*/SWNT/4-ATP/Au in phosphate buffer solution.

5.3.2.4 Electrocatalysis of SWNT-Cyt *c* Electrodes to the Reduction of Hydrogen Peroxide

In order to characterize the functionalized Cyt *c* electrodes, the electrocatalytic activity towards hydrogen peroxide (H_2O_2) has been studied in phosphate buffer solution under N_2 atmosphere. Figure 17 shows the cyclic voltammograms of Cyt *c*-SWNT on 4-ATP with successive addition of hydrogen peroxide to the phosphate buffer solution of pH 6.5. With increasing the H_2O_2 concentration the reduction current increases. Chronoamperometry measurements were carried out to study the electrocatalysis of Cyt *c*-SWNT. They have been conducted at ambient, stirred conditions in phosphate buffer solution of pH 6.5, at -110 mV. The CA results clearly shows the functionalization of SWNT with Cyt *c* has not altered the surface activity of the redox protein. Figure 18(I) shows the amperometric responses of 4-ATP modified and Cyt *c*-SWNT modified electrodes with successive addition of H_2O_2. Upon addition of an aliquot of H_2O_2 to the buffer solution, the reduction current increases steeply to reach a steady state value within 5 seconds.

The concentration of H_2O_2 is increased in steps of 3.8 mM. The Cyt *c*-SWNT electrode shows higher catalytic activity compared to the Cyt *c* modified 4-ATP electrode (without SWNTs). The higher catalytic activity in the presence of SWNTs may be attributed to the SWNTs functioning as molecular wire for the electron transport from the protein redox center to the electrode surface. Figure 18(II) shows the calibration plots for Cyt *c*-SWNT immobilized on 4-ATP covered gold electrodes. Linear calibration plots are obtained for the electrodes in the concentration range of 3.8 mM to 34.2 mM. The detection limit was found to be 200 μM.

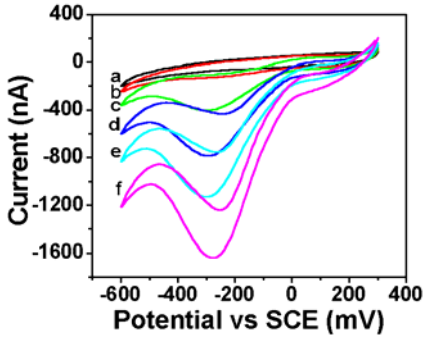

Figure 17. Cyclic voltammograms showing the reduction of H_2O_2 at different concentrations for Cyt *c*/SWNT/4-ATP/Au electrode in phosphate buffer solution of pH 6.5 under N_2 atmosphere at a scan rate of 50mVs^{-1}. The concentration of H_2O_2 a) 0 mM, b) 3.8 mM, c) 7.6 mM, d) 11.4 mM, e) 15.2 mM and f) 19 mM.

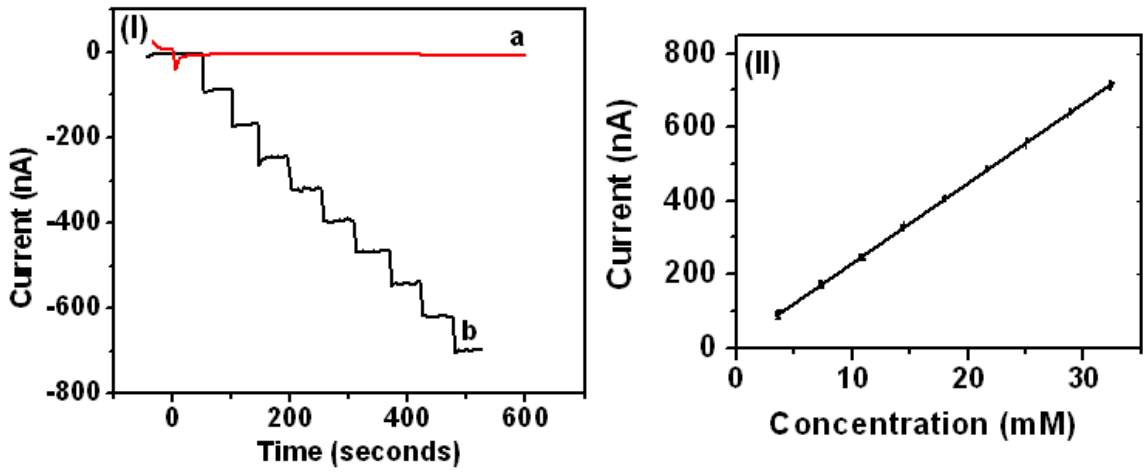

Figure 18. (I) Amperometric response to H_2O_2 with successive addition of 3.8 mM H_2O_2 under stirred conditions in a phosphate solution of pH 6.5 under N_2 atmosphere. a) 4-ATP/Au, b) Cyt *c*/SWNT/4-ATP/Au. Applied potential was –110 mV. (II) Calibration plot of Cyt *c*-SWNTs.

5.3.3 Electron Transfer and Electrocatalysis of Electrochemically Immobilized Cyt *c* and Cyt *c*-SWNT on Self-Assembled Monolayer of 4-ATP

The interfacial properties of protein on the surfaces depend on the immobilization technique. Unlike the earlier method of simple immersion deposition, here we have immobilized the protein electrochemically at ambient temperature. The protein Cyt *c* was immobilized on the SAM of 4-ATP by potential cycling between -500 to +500 mV in Cyt *c* solution for about 50 cycles. The protein is non-covalently immobilized by this process by predominantly hydrophilic interaction between hydrophilic outer surfaces of the Cyt *c* and 4-ATP.

We have studied the direct electron transfer and mediator free amperometric hydrogen peroxide biosensor that employs an electrochemically immobilized surface active Cyt *c* on aromatic self-assembled monolayers of 4-ATP. The results demonstrate the high sensitivity to H_2O_2 reduction in the buffer medium. Furthermore, the amperometric response of the Cyt *c* modified electrodes was enhanced significantly using SWNTs.

5.3.3.1 Atomic Force Microscopy Studies

The protein modified surfaces were characterized by tapping mode atomic force microscopy. Figure 19a and 19b shows the AFM image of 4-ATP monolayer on gold and electrochemically immobilized Cyt *c* on 4-ATP surface (ECyt *c*/4-ATP/Au). The image 19b shows that the protein

clusters are distributed in the entire region of the scanned area which are absent in the case of 4-ATP modified surface. The height and widths of clusters varies from one cluster to the other. The heights are in the range of 30-120 nm and widths are in the range of 50 nm to a few microns. Figure 20 shows the phase image of electrochemically immobilized Cyt *c*-SWNT on 4-ATP modified gold surface. The image shows the densely coated protein immobilized on SWNTs on the 4-ATP modified surface.

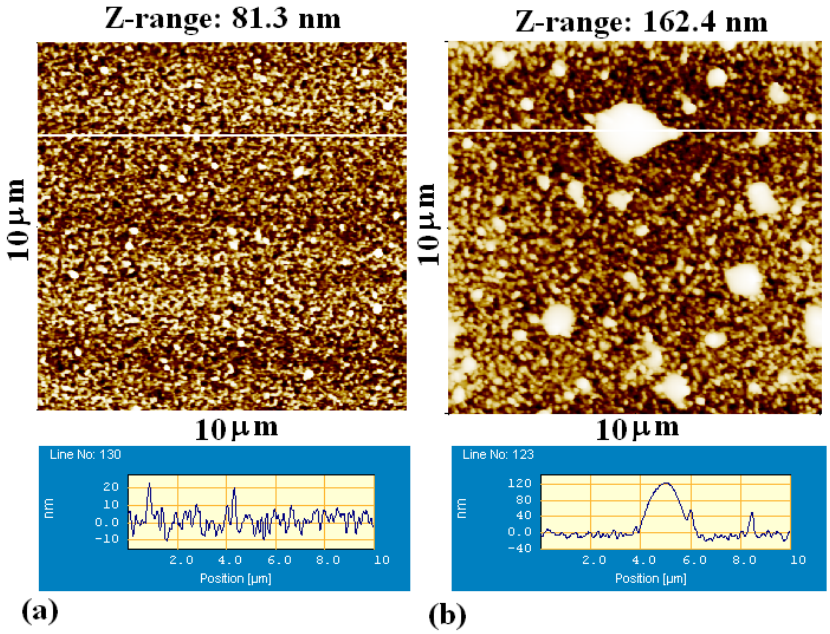

Figure 19. AFM image of (a) 4-ATP/Au (b) ECyt *c*/4-ATP/Au.

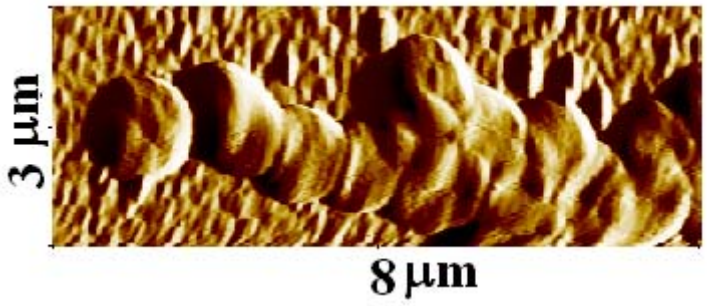

Figure 20. AFM phase image of ECyt *c*/SWNT/4-ATP/Au.

5.3.3.2 Cyclic Voltammetry Studies

Figure 21(I) shows the cyclic voltammetry of 4-ATP modified gold electrode in Cyt *c* solution with different scan rates. A pair of quasi-reversible redox peaks was observed in Cyt *c* solution.

The anodic and cathodic peak currents increase linearly with the square root of scan rate as shown in the Figure 21(II), which indicates that diffusion controlled process.

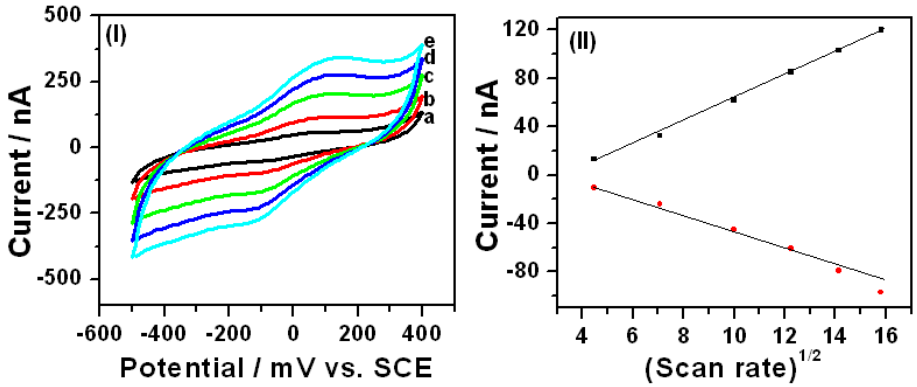

Figure 21. (I) Cyclic voltammograms of 4-ATP/Au electrode in Cyt *c* solution of pH 6.5 under N_2 atmosphere at scan rate (mV s^{-1}) of (a) 20, (b) 50, (c) 100, (d) 150, and (e) 200. (II) The plot of peak current verses square root of scan rate.

Figure 22(I) shows cyclic voltammograms of the electrochemically immobilized Cyt *c*-SWNT on 4-ATP modified gold surface in a phosphate buffer solution at different scan rates. The cyclic voltammograms shows redox peaks corresponding to the Fe^{2+}/ Fe^{3+} of immobilized Cyt *c*. The peak current varies linearly with scan rate following the expression $i_p = n^2F^2\nu A\Gamma/4RT$, where n=number of electrons, F=Faraday constant, Γ=the number of redox active sites on the surface, A=area, ν=scan rate as shown in the Figure 22(II), indicating a diffusionless surface bound species.

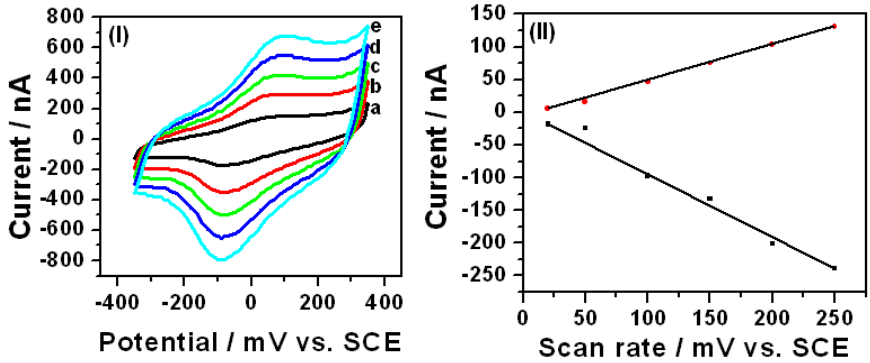

Figure 22. (I) Cyclic voltammograms of ECyt *c*/SWNT/4-ATP/Au electrode in 0.1 M phosphate buffer solution of pH 6.5 under N_2 atmosphere at scan rates (mVs^{-1}) of (a) 20, (b) 50, (c) 100, (d) 150, and (e) 200. (II) The plot of peak current verses scan rate.

5.3.3.3 Chronoamperometry Studies

The electrocatalytic reduction of H_2O_2 at protein modified surface was studied by chronoamperometry. The chronoamperometry measurements were conducted at ambient temperature in phosphate buffer solution of pH 7.0 under N_2 atmosphere with constant stirring at -110 mV verses SCE, and the catalytic reduction currents were measured. Figure 23(I) shows the amperometric response of Cyt *c* and Cyt *c*-SWNT electrodes. The concentration of H_2O_2 is increased in steps of 86 μM. Current due to H_2O_2 reduction is considerably higher in the case of the electrode containing SWNT covered with Cyt *c* compared to the Cyt *c* on 4-ATP. Detection limits for H_2O_2 were determined by adding very small amounts of H_2O_2 until there is a detectable (few nA) change in current. The steady state current observed was significantly higher compared to the background noise. The detection limits were found to be 40 μM for the Cyt *c* modified and 10 μM for the Cyt *c*-SWNT modified electrodes respectively. Linear calibration plots were obtained for the electrodes in the concentration range of 86 μM to 774 μM as shown in the inset of Figure 23(II).

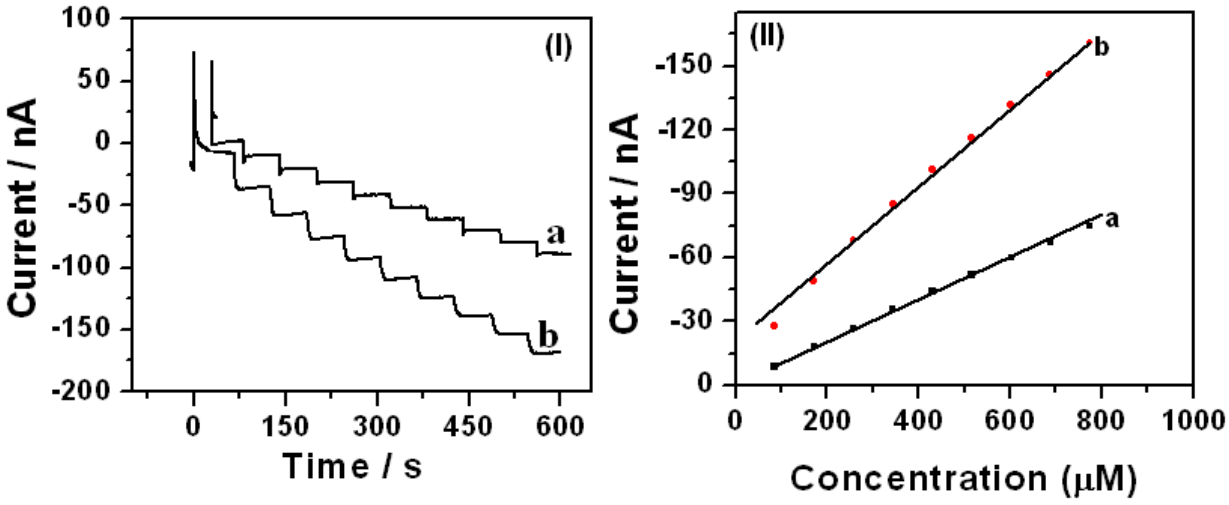

Figure 23. (I) Chronoamperometry measurements of Cyt *c* modified electrodes (a) ECyt *c*/4-ATP/Au and (b) ECyt *c*-SWNT/4-ATP/Au electrodes with successive addition of H_2O_2 in phosphate buffer solution (PBS) of pH 7.0 under N_2 atmosphere and stirred conditions (II) Corresponding calibration plots.

5.3.4 Electron Transfer and Electrocatalysis of Cyt *c* and Cyt *c*-SWNT on 4-Mercaptobenzoic Acid (4-MBA) Self-Assembled Monolayers

The immobilizations of proteins on self-assembled monolayers depend on the type of the monolayer used. In the previous section, we have described the immobilized protein on 4-aminothiophenol (4-ATP) monolayer formed by covalently, non-covalently, and electrochemically. The Cyt *c*-SWNT composites were prepared non-covalently and electrochemically on 4-ATP at pH 7. In this section, we have discuss the results on Cyt *c* on negatively charged 4-MBA. Cyt *c* and Cyt *c*-SWNT immobilized surfaces were studied for their electrocatalytic properties. The protein modified surfaces were characterized by atomic force microscopy.

5.3.4.1 AFM Studies

Figure 24a is the noncontact mode AFM image of the Cyt *c*-SWNT immobilized non-covalently on 4-MBA modified gold surface. The image shows that the clusters of proteins are present along with the SWNTs. The heights of clusters are in the range of 10-80 nm. Figure 24b shows the individual cluster of Cyt *c* wrapped SWNTs. The heights of the clusters are around 30 nm. Since the modified protein molecules have the dimensions of 4-5 nm it is inferred that the multilayer adsorption of protein takes place on the SWNTs. The length of this cluster is about 2 μm. The extended length of the protein covered SWNTs is due to the parallel alignment of protein covered SWNTs similar to the Cyt *c*-SWNTs composites on 4-ATP modified gold surface discussed above. Figure 25a shows the AFM image of the electrochemically immobilized Cyt *c* on 4-MBA. Here, size of the protein clusters are bigger than that of Cyt *c*-SWNT immobilized non-covalently by simple adsorption. SWNTs are completely covered by protein which makes it difficult for the SWNTs to be distinguishable from the protein molecules. However, phase image shows the clearly resolved the bundles of SWNTs along with the protein clusters as seen in the Figure 25b.

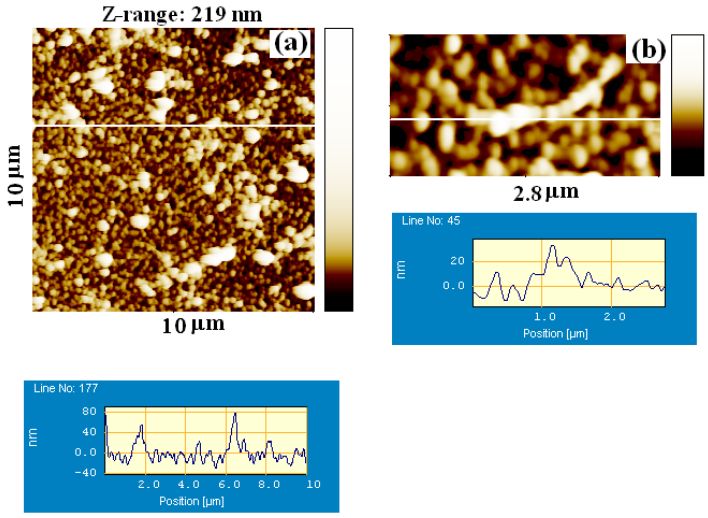

Figure 24. AFM image of the Cyt *c*-SWNT immobilized on 4-MBA (a) 10 x 10 µm image (b) another region of the scanned area.

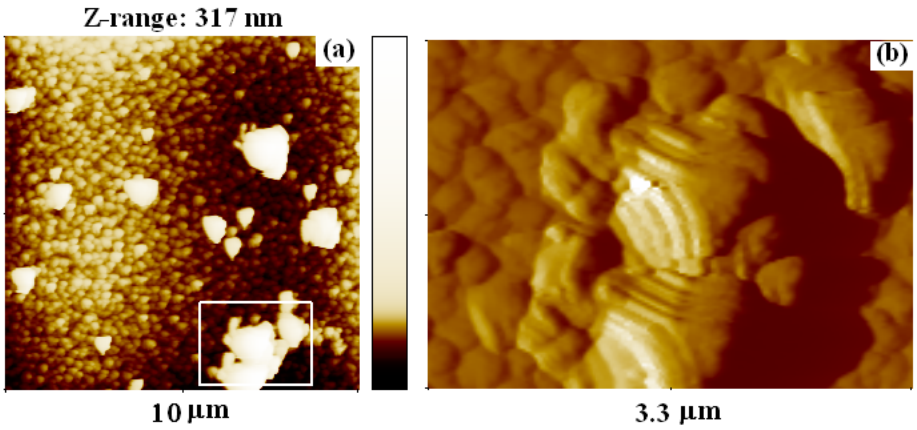

Figure 25. AFM image of the electrochemically immobilized Cyt *c*-SWNT on 4-MBA (a) topographic image (b) phase image of the zoomed portion of 23a.

5.3.4.2 Chronoamperometry Measurements

The electrocatalytic reduction of H_2O_2 at protein modified surface was studied by chronoamperometry. The chronoamperometry measurements were conducted at ambient temperature in phosphate buffer solution of pH 7.0 under N_2 atmosphere with constant stirring. The amperometric response of protein modified electrodes was recorded at -110 mV verses SCE and the catalytic reduction currents were measured. Figure 26(I) shows the amperometric response of Cyt *c* immobilized covalently, non-covalently, and electrochemically on 4-MBA modified surface. The concentration of H_2O_2 was increased in steps of 8.8 x 10^{-4} M. Figure 26(II)

shows the corresponding calibration plot. Linear calibration curves were obtained in the concentration range 8.8 – 79.2 x 10^{-4} M. The H_2O_2 reduction current is higher for non-covalent immobilized Cyt *c* compared to the covalent immobilized electrode. This is due to higher protein content in the case of non-covalent immobilized electrode. The current due to electrochemically immobilized electrodes is higher compared to the covalent and non-covalent immobilized electrodes. Higher current may be due to the higher protein content of the electrochemically immobilized Cyt *c* on 4-MBA compared to the covalent and non-covalent immobilized electrodes.

Current due to H_2O_2 reduction is considerably higher in the case of the electrode containing Cyt *c* covered SWNT compared to the Cyt *c* alone on 4-MBA. Figure 27(I) shows the amperometric responses for the Cyt *c*-SWNT immobilized by simple adsorption and electrochemical adsorption. Figure 27(II) shows the corresponding calibration plots. Linear calibration curves were obtained in the concentration range 8.8 – 79.2 x 10^{-4} M. The detection limits were found to be 40 μM for the Cyt *c* modified and 10 μM for the Cyt *c*-SWNT modified electrodes respectively.

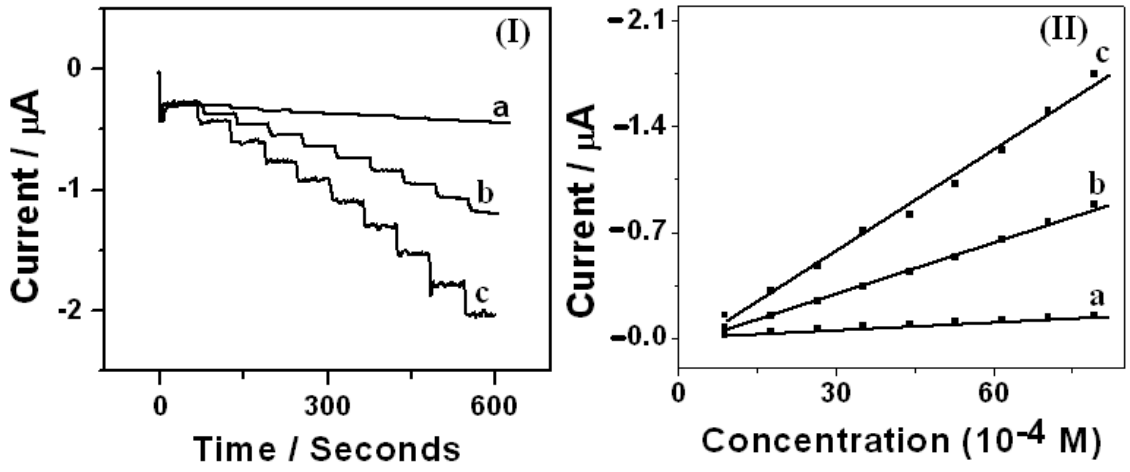

Figure 26. (I) Chronoamperometry measurements of Cyt *c* modified electrodes (a) Cyt *c*/GA/4-MBA/ Au, (b) Cyt *c*/4-MBA/Au, (c) ECyt *c*/4-MBA/Au electrodes with successive addition of H_2O_2 in phosphate buffer solution (PBS) of pH 7.0 under N_2 atmosphere and stirred conditions (II) Corresponding calibration plots.

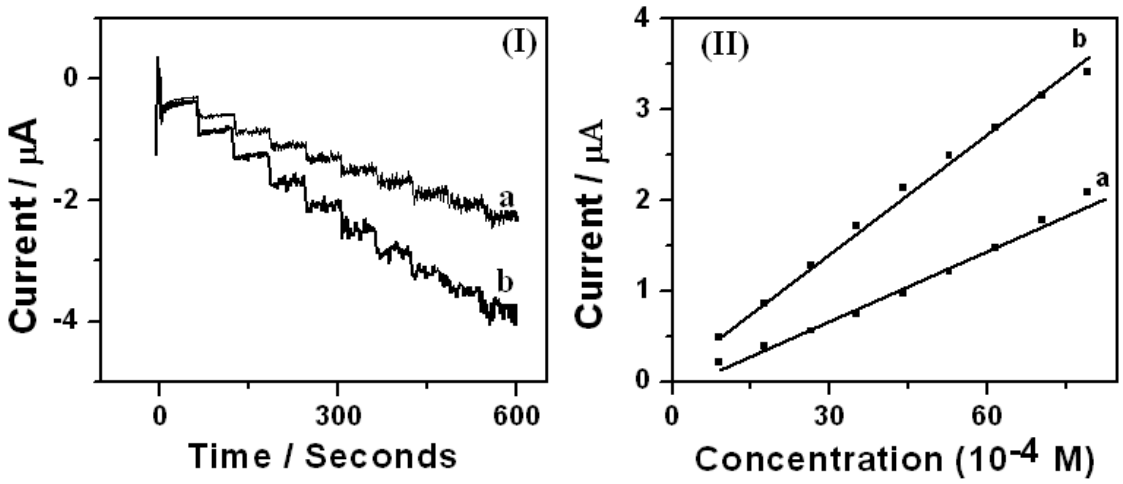

Figure 27. (I) Chronoamperometry measurements of Cyt *c* modified electrodes (a) Cyt *c*-SWNT/4-MBA/Au and (b) ECyt *c*-SWNT/4-MBA/Au electrodes with successive addition of H_2O_2 in phosphate buffer solution (PBS) of pH=7.0 under N_2 atmosphere and stirred conditions (II) Corresponding calibration plots.

5.3.5 Immobilization and Studies of Myoglobin and Myoglobin-SWNT Composites on Aromatic Self-Assembled Monolayers of 4-ATP

Myoglobin is heme protein having molecular weights 17, 800 Daltons. Myoglobin functions as storage of oxygen and facilitates the transport of oxygen to the mitochondria [68-69]. Myoglobin consists of a single polypeptide chain of about 153 amino acids [70-73]. Inside protein consists of nonpolar residues including leucine, valine, methionine, and phenylalanine. Polar residues such as aspartate, glutamate, lysine, and arginine are absent from the interior protein surface [74].

Myoglobin (Myb) is a redox active protein, has an isoelectric point of 7.1 and catalyzes hydrogen peroxide reduction. Although, Myb does not function in biological electron transfer chains, it is known for its peroxidase catalytic activity [75-76]. There are several reports of the study of direct electron transfer and electrocatalysis of myoglobin on self-assembled monolayers, gold nanoparticles, surfactant films and carbon nanotubes [77-84]. Generally immobilization of proteins on self-assembled monolayers is carried out by non-covalent binding through hydrophilic or hydrophobic interactions or covalent binding using suitable linker molecules [85-88].

Here, we have exploited the hydrophilic property of the self-assembled monolayer of 4-aminothiophenol (4-ATP) on gold, which helps to bind myoglobin, which has a hydrophilic outer surface. To enhance the electrocatalytic activity of proteins, we have also immobilized the Myb-SWNT composites and studied their electrocatalytic activities using electrochemical techniques.

5.3.5.1 AFM and STM Studies

The tapping mode AFM images of Figures 28A and 28B show respectively the bare gold and the myoglobin immobilized on 4-ATP modified electrode. The AFM image of 4-ATP modified gold surface is indistinguishable from the bare gold surface (not shown here). The image in Figure 28C shows that the myoglobin immobilized by electrochemical cycling on 4-ATP gold surface. It can be seen that in the case of electrochemical cycling, myoglobin is adsorbed densely on several regions of the surface of 4-ATP on gold surface. The sizes of these are of few hundreds of nm while the heights are more than the myoglobin immobilized by simple immersion process, as shown in the line scans of Figure 28B and 28C. Figure 29a shows the STM image of the immobilized myoglobin on the surface of 4-ATP modified gold surface by simple immersion process. This is a representative image at one of the scanned locations. The small clusters of protein molecules are adsorbed on the surface forming a stripped pattern. The magnified image of the same surface in Figure 29b obtained when scanned in a lower range clearly shows that these clusters are constituted of individual protein molecules with a size of about 3 – 4 nm. Figure 29c shows the STM image of the surface where the myoglobin was immobilized on the surface by potential cycling by cyclic voltammetry which again shows a dense and rather periodic arrangement of Myb on 4-ATP modified gold surface.

Figure 30a and 30b show respectively the AFM images of Myb-SWNT composite modified 4-ATP electrodes formed by non-covalent adsorption (Figure 30a) and by electrochemical cycling (Figure 30b). There are several rod like features in Figure 30(a) and (b). These features suggest that the protein wrapped single walled carbon nanotubes bundles are aggregated to form dense clusters in several regions.

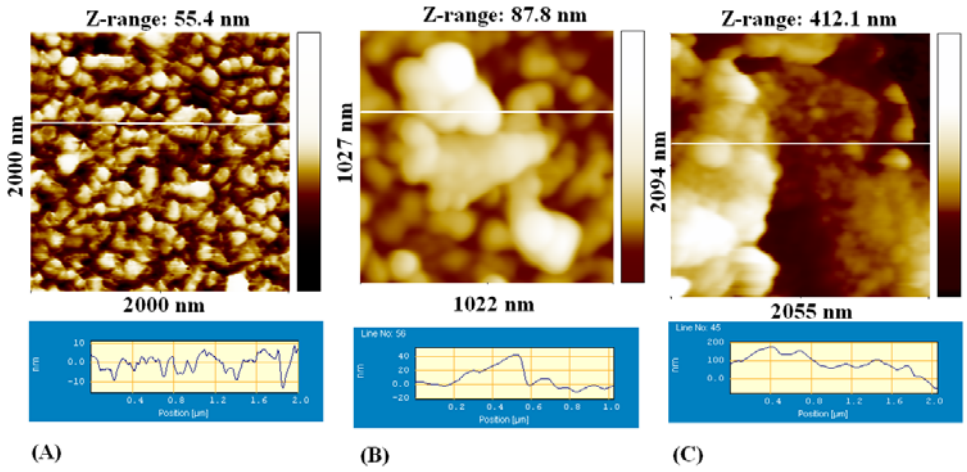

Figure 28. AFM images of A) Au B) Myb/4-ATP/Au, and C) EMyb/4-ATP/Au surfaces. The line scans are shown below the corresponding images.

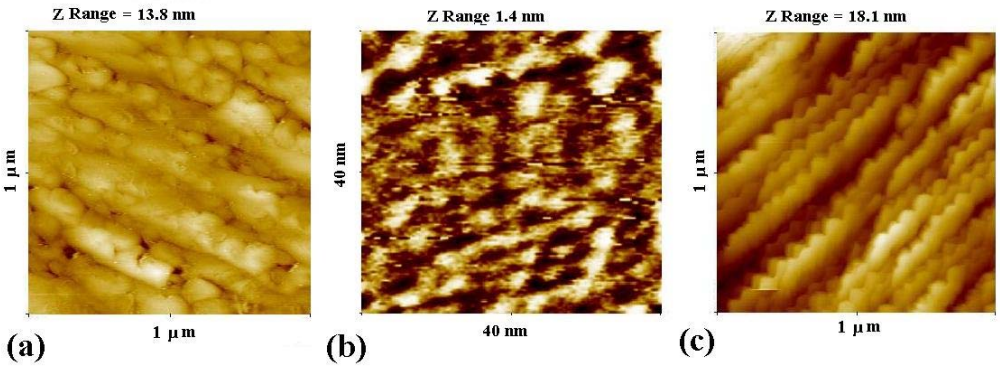

Figure 29. STM image of (A) Myb/4-ATP/Au, (B) Zoomed portion, and (C) EMyb/4-ATP/Au.

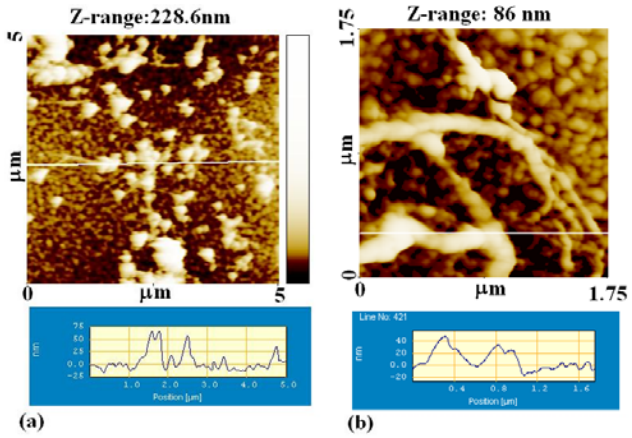

Figure 30. AFM images of (a) Myb-SWNT/4-ATP/Au surface and (b) EMyb/SWNT/4-ATP/Au surface and corresponding line scans are shown below the images.

5.3.5.2 Cyclic Voltammetry Studies

To characterize the Myb modified electrodes, CV studies have been carried out using $K_4Fe(CN)_6$ as a redox probe. Figure 31(I) (inset) shows the CV of bare Au in 10 mM of $K_4Fe(CN)_6$ solution containing 1 M NaF as supporting electrolyte. Figure 31(I) shows 4-ATP modified Au electrode and Myb modified electrodes in the same medium. Figure 31(II) shows 4-ATP modified Au electrode and Myb-SWNT modified electrodes in 10 mM of $K_4Fe(CN)_6$ solution containing 1 M NaF as supporting electrolyte. It can be seen that bare gold electrode shows reversible peaks, which indicates efficient electron transfer processes (inset of Figure 31(I)). The electron transfer for the 4-ATP modified electrode shows quasi reversible peaks with a peak separation of 200 mV. The barrier towards the electron transfer of $K_4Fe(CN)_6$ is further increased in the case 4-ATP modified Myb surfaces indicating the formation of protein film on 4-ATP. The electron transfer reaction of $K_4Fe(CN)_6$ is almost completely hindered in the case of Myb immobilizied electrochemically on 4-ATP. This is due to the formation of dense protein film on 4-ATP in the case of electrochemically immobilized Myb as also confirmed by AFM studies (Figure 28(c)). The electron transfer reaction of $K_4Fe(CN)_6$ on Myb-SWNT modified electrodes is less inhibited than the Myb modified surfaces. This is attributed to the higher rate of electron transfer through Myb-SWNT composite with SWNTs acting as a molecular wire for the electron transfer.

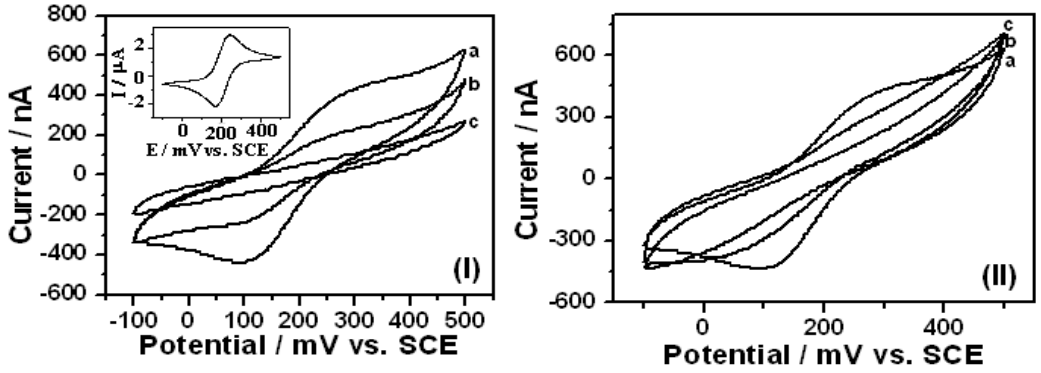

Figure 31. CV taken in 10 mM $K_4Fe(CN)_6$ solution containing 1 M NaF as supporting electrolyte. (I) (a) 4-ATP modified Au, (b) Myb/4-ATP/Au, (c) electrochemically cycled Myb/4-ATP/Au and (II) (a) 4-ATP modified Au, (b) Myb-SWNT/4-ATP/Au, and (c) electrochemically cycled Myb-SWNT/4-ATP/Au. Inset of Figure 31(I) shows bare Au CV in $K_4Fe(CN)_6$.

The cyclic voltammetry has been used to study the direct electron transfer properties of Myb immobilized electrode. The cyclic voltammetry was carried out in a phosphate buffer solution of pH 7.0 under N_2 atmosphere. Figure 32 shows the cyclic voltammogram of Myb modified 4-ATP electrode. The CVs show redox peaks corresponding to the Fe^{2+}/Fe^{3+} reaction. From the voltammograms at different scan rates, the electron transfer rates were calculated using Laviron model [89]. The electron transfer rate constant measured for the system is $0.7s^{-1}$ which is comparable with the reported value for Myb [80]. The redox peak currents (i_p) of immobilized Myb on SAM increases linearly with scan rate (ν) as shown in the inset of Figure 32 following the expression $i_p = n^2F^2\nu A\Gamma/4RT$, where n=number of electrons, F=Faraday constant, Γ=the number of redox active sites on the surface, A=area, ν=scan rate. The linearity of the plot indicates a diffusionless surface confined electron transfer processes.

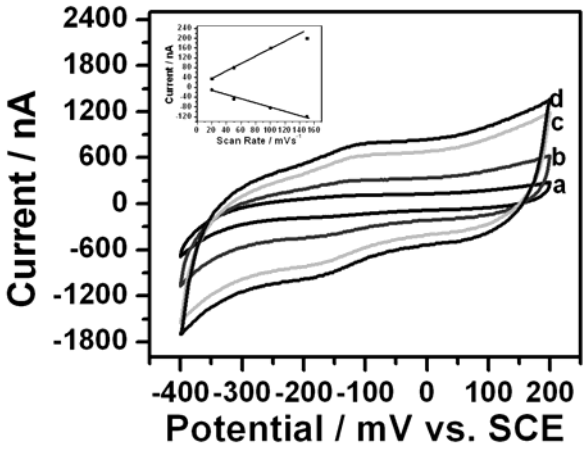

Figure 32. CV of Myb/4-ATP/Au taken in 100 mM phosphate buffer solution (PBS) of pH=7.0 under N_2 at different scan rates (mV/s) a) 20, b) 50 c) 100 and d) 150. Inset shows the plot of peak current versus scan rate.

5.3.5.3 Electrocatalytic Activity Towards Hydrogen Peroxide (H_2O_2)

Heme proteins such as cytochrome *c*, hemoglobin, horseradish peroxidase and myoglobin have been known to catalyze the reduction of H_2O_2. This aspect is studied for the Myb modified electrode.

5.3.5.3.1 Cyclic Voltammetry Studies

To evaluate the bioelectrocatalytic activity of Myb modified and Myb-SWNT composite electrodes, the electrochemical reduction of hydrogen peroxide has been studied using cyclic voltammetry in phosphate buffer solution of pH 7.0. Figure 33 shows the cyclic voltammograms of Myb modified 4-ATP electrodes in 100 mM phosphate buffer solution of pH 7.0 at different concentration of H_2O_2. Figure 33(I) shows the electrocatalytic response of the myoglobin modified electrode, Figure 33(II) is that of the electrode after potential cycling. It is clear that the potential cycling has enhanced the catalytic response of the modified electrode. The CVs of the Myb-SWNT composite electrode are shown in Figure 34(I) while Figure 34(II) shows that of the potential cycled electrode. Here too the response shows that the potential cycling has enhanced the electrocatalytic activity. The concentration of H_2O_2 was increased in steps of 44 x 10^{-5} M. It can be seen that the reduction currents increase correspondingly. These results clearly demonstrate the catalytic reduction of H_2O_2 by myoglobin and Myb-SWNT composite modified 4-ATP electrodes. This clearly due to the higher protein content of electrochemically immobilized surfaces.

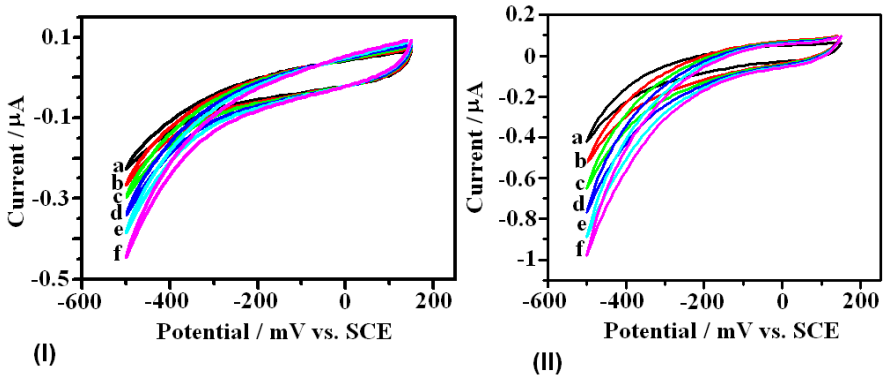

Figure 33. CVs of (I) Myb/4-ATP/Au and (II) EMyb/4-ATP/Au in 100 mM phosphate buffer solution (PBS) of pH 7.0 under N_2 atmosphere with addition of H_2O_2 a) 0 M, b) 44 x 10^{-5} M, c) 88 x 10^{-5} M, d) 132 x 10^{-5} M, e) 176 x 10^{-5}M, and f) 220 x 10^{-5}M.

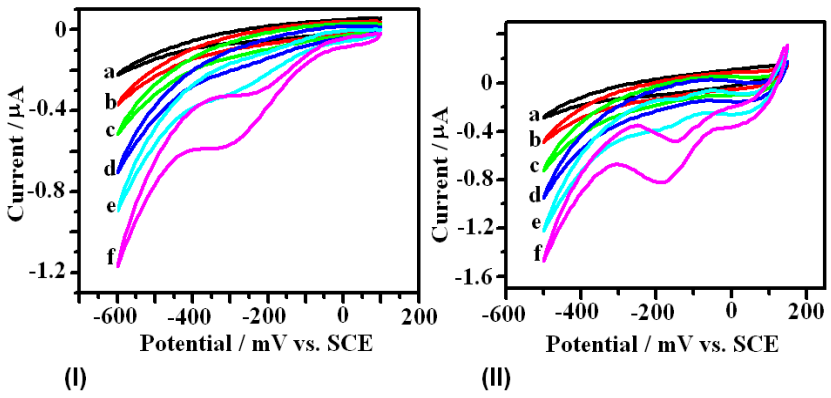

Figure 34. CVs of (I) Myb-SWNT/4-ATP/Au and (II) EMyb-SWNT/4-ATP/Au in 100 mM phosphate buffer solution (PBS) of pH 7.0 under N_2 atmosphere with addition of H_2O_2 a) 0 M, b) 44 x 10^{-5} M, c) 88 x 10^{-5} M, d) 132 x 10^{-5} M, e) 176 x 10^{-5}M, and f) 220 x 10^{-5}M.

5.3.5.3.2 Chronoamperometric Measurements

Amperometric responses of the myoglobin on the self-assembled monolayers on 4-ATP electrodes have been recorded with successive addition of hydrogen peroxide by continuously stirring the phosphate buffer solution under N_2 atmosphere.

The chronoamperometric measurements were carried out at different applied potentials and the electrochemical reduction of H_2O_2 has been studied from –100 mV to –600 mV verses SCE in steps of 100 mV. We find that the current increases with the applied potential and reaches saturation value beyond -500 mV.

Figure 35(I-II) shows the chronoamperometic response of 4-ATP modified gold electrode, myoglobin modified 4-ATP and Myb-SWNT modified 4-ATP electrodes respectively for successive additions of hydrogen peroxide at -500 mV. It is also seen that in both the cases the electrochemically cycled electrodes as in Figure 35I(c) and 35II(c) show higher current response compared to the electrodes in which the myoglobin or Myb-SWNT is immobilized by simple immersion as in Figure 35I(b) and 35II(b). It can be seen that with increasing H_2O_2 concentration, the bioelectrochemical reduction current of H_2O_2 increases. However, direct reduction of H_2O_2 was negligible at 4-ATP modified electrode in comparison to the Myb and Myb-SWNT composite modified electrodes as shown in the Figure 35I(a) and 35II(a).

Detection limits for H_2O_2 were determined by adding very small amounts of H_2O_2 until there is a detectable (few nA) change in current. The steady state current observed was about 4 times the background noise. The detection limits were found to be 200 µM for the myoglobin

modified and 150 μM for the Myb-SWNT modified electrodes respectively. The detection limits were found to be 115 μM and 108 μM for the respective electrochemically cycled electrodes.

The inset of Figure 35 shows the calibration plots for myoglobin modified 4-ATP and Myb-SWNT modified 4-ATP surfaces, respectively. Linear response is obtained over almost a decade change in the concentration from 4.40 x 10^{-4} M to 3.96 x 10^{-3} M.

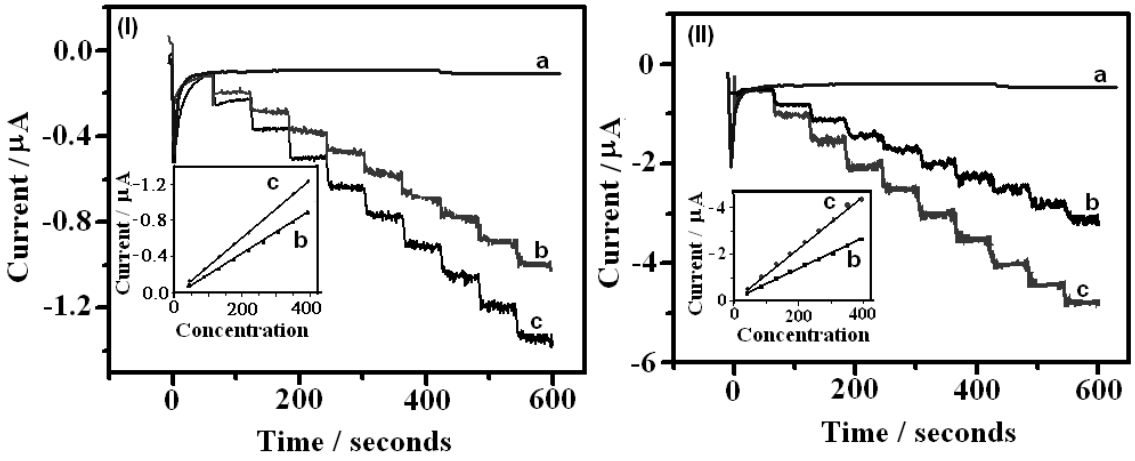

Figure 35. Chronoamperometric measurements of Myb and Myb-SWNT modified electrodes. (I) (a) 4-ATP/ Au, (b) Myb/4-ATP/Au, and (c) EMyb/4-ATP/Au and (II) (a) 4-ATP/ Au, (b) Myb-SWNT/4-ATP/Au, and (c) EMyb-SWNT/4-ATP/Au electrodes with successive addition of 44 x 10^{-5} M of H_2O_2 in phosphate buffer solution (PBS) of pH 7.0 under N_2 atmosphere under stirred conditions in 100 mM PBS. Inset shows the calibration plots.

5.3.6 Immobilization and Studies of Horseradish Peroxidase and Horseradish peroxidase-SWNT on Self-Assembled Monolayers

Horseradish peroxidase (HRP) is a 44,173.9 dalton protein. HRP is a single chain polypeptide containing four disulfide bridges. The 18% carbohydrate is constituted of galactose, arabinose, xylose, fucose, mannose, mannosamine, and galactosamine depending upon the specific isozyme. The isoelectric point of HRP is around 6.8 [90].

HRP readily combines with hydrogen peroxide (H_2O_2) and the resultant [HRP-H_2O_2] complex can oxidize a wide variety of hydrogen donors. HRP is ideal in many applications because it is more stable and less expensive than other popular alternatives such as alkaline

phosphatase. It also has a high turnover rate that allows generation of strong signals in a relatively short time span.

Horseradish peroxidase (HRP), functioning physiologically as in the biocatalysis of H_2O_2, has been extensively investigated. The direct electron transfer catalysis of immobilized HRP has been achieved on different modified surfaces [91-94]. There are some reports in literature on HRP-SWNT modified electrodes [95-98].

5.3.6.1 AFM Studies

Figure 36 shows the AFM image of the HRP-SWNT on 4-ATP modified gold surface. There are rod like features, with heights which are in the range 10-30 nm. These features clearly show that the HRP wrapped SWNTs has been immobilized on the surface. The heights of more than 10 nm implies that multilayer of protein molecules was formed on the surface.

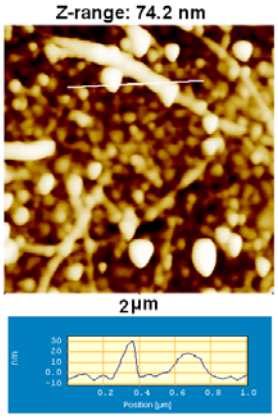

Figure 36. AFM image of the HRP-SWNT immobilized on 4-ATP modified Au surface.

5.3.6.2 Redox Properties

Figure 37 shows the HRP-SWNT cyclic voltammograms taken in a phosphate buffer solution at different scan rates immobilized on 4-ATP modified gold surface. The cyclic voltammograms shows redox peaks corresponds to Fe^{2+}/ Fe^{3+} reaction of immobilized HRP. The peak current varies linearly with scan rate following the expression $i_p = n^2F^2\nu A\Gamma/4RT$, where n=number of electrons, F=Faraday constant, Γ=the number of redox active sites on the surface, A=area, ν=scan rate as shown in the Figure 37(II), indicating a diffusionless surface bound species. The half peak potential for the electron transfer process is -110 mV verses SCE.

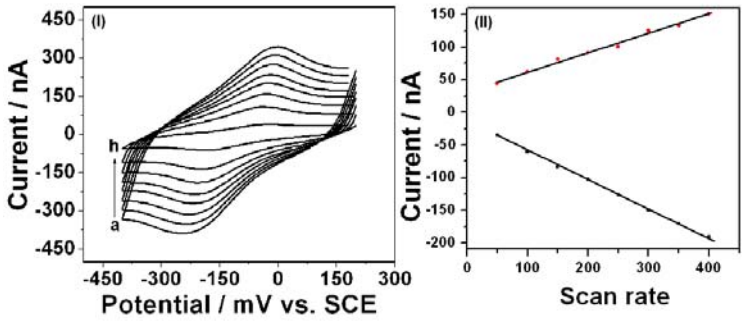

Figure 37. (I) Cyclic voltammograms of HRP/SWNT/4-ATP/Au electrode in 0.1 M phosphate buffer solution of pH 6.5 under N_2 atmosphere at scan rates (mVs^{-1}) of (a) 50, (b) 100, (c) 150, (d) 200, (e) 250, (f) 300, (g) 350, and (h) 400 (II) The plot of Peak current verses scan rate.

5.3.6.3 Electrocatalysis of HRP and HRP-SWNT Modified Electrodes Towards the Reduction of Hydrogen Peroxide (H_2O_2)

The electrocatalytic reduction of H_2O_2 at protein modified surface was studied using CA. The CA measurements were conducted at ambient temperature in phosphate buffer solution of pH 7.0 under N_2 atmosphere with constant stirring. The amperometric response of protein modified electrodes was recorded as -250 mV. This potential was chosen based on the CVs for the H_2O_2 reduction at HRP modified surfaces, which exhibits the reduction peak of H_2O_2 at -250 mV. Figure 38A is the amperometric response of HRP immobilized by covalent, non-covalent and electrochemical methods on 4-ATP. The concentration of H_2O_2 was increased in steps of 25 μM. The current due to H_2O_2 reduction is considerably higher in the case of electrochemically immobilized HRP compared to the covalent and non-covalent methods. Detection limits for H_2O_2 were determined by adding very small amounts of H_2O_2 until there is a detectable (few nA) change in current. The detection limits were found to be 10, 1, and 0.8 μM for covalent, non-covalent and electrochemically immobilized electrodes, respectively. Linear calibration plots were obtained in the concentration range of 50 μM to 275 μM as shown in the Figure 38B.

Figure 39A is the amperometric response of HRP-SWNT immobilized on 4-ATP. The concentration of H_2O_2 was increased in steps of 25 μM. Current due to H_2O_2 reduction is considerably higher in the case of electrochemically immobilized HRP-SWNT compared to the simple adsorption of HRP-SWNT on 4-ATP surface. The detection limits were found to be 0.09 and 0.05 μM for HRP-SWNT and EHRP-SWNT electrodes, respectively. Linear calibration plots are obtained in the concentration range of 50 μM to 225 μM as shown in Figure 39B.

Table 2 shows the detection limits for the different proteins immobilized on 4-ATP monolayer. It can be seen from the table that HRP shows very low detection limits compared to the Cyt c and Myb. This shows that the HRP posses the highest catalytic activity for H_2O_2 reduction among the three redox proteins studied in this work. The results also establishes the catalytic activity of all the proteins are significantly enhanced by functionalizing with SWNTs.

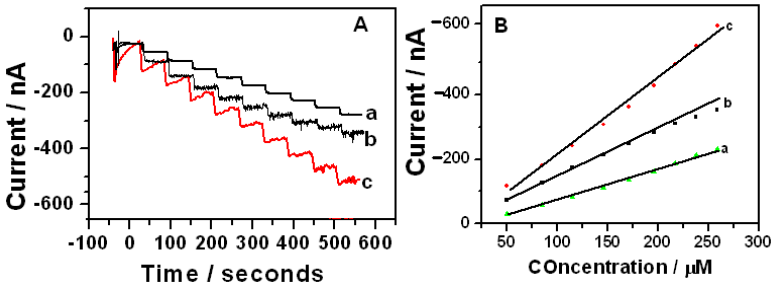

Figure 38. (A) Chronoamperometry measurements of HRP modified electrodes (a) HRP/GA/4-ATP/ Au, (b) HRP/4-ATP/Au, and (c) EHRP/4-ATP/Au electrodes with successive addition of H_2O_2 in phosphate buffer solution (PBS) of pH 7.0 under N_2 atmosphere and stirred conditions (B) corresponding calibration plots.

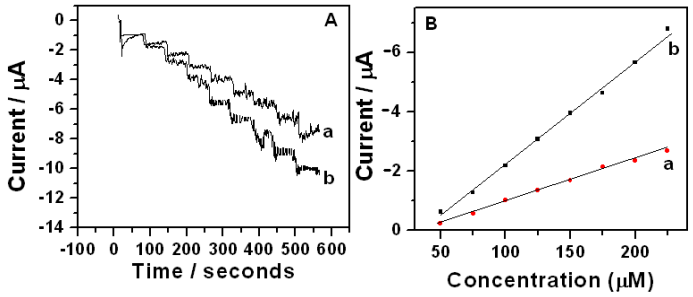

Figure 39. (A) Chronoamperometry measurements of HRP-SWNT modified electrodes (a) HRP-SWNT/4-ATP/ Au and (b) EHRP-SWNT/4-ATP/Au electrodes with successive addition of H_2O_2 in phosphate buffer solution (PBS) of pH 7.0 under N_2 atmosphere and stirred conditions (B) corresponding calibration plots.

Protein	Cyt c (μM)	Myb (μM)	HRP (μM)
Covalent	800	-	10
Non-covalent	400	200	1
Electrochemical	40	115	0.8
Non-Covalent (protein-SWNT)	200	150	0.09
Electrochemical (protein-SWNT)	10	108	0.05

Table 2. Shows the detection limits for hydrogen peroxide reduction catalyzed by different proteins immobilized on 4-ATP.

5.4 Conclusions

The self-assembled monolayers formed by the chemisorption of thiols on gold offers a platform for immobilization of proteins on surfaces while simultaneously retaining the bioactivity. The electrocatalytic activity of proteins on surfaces depends on the immobilization technique. We have immobilized the proteins by different methods such as covalent coupling, non-covalent adsorption and by electrochemical cycling on self-assembled monolayers. To enhance the electrocatalytic activity of proteins on surfaces, composites of protein-SWNTs have been immobilized non-covalently by simple immersion process and electrochemically by potential cycling the monolayer modified electrode in protein-SWNT composites. The proteins which have been studied are Cytochrome *c*, Myoglobin, and Horseradish peroxidase. The electrochemical studies have been carried out using cyclic voltammetry, electrochemical impedance spectroscopy, and chronoamperometry. The measured rate constant for the covalently immobilized Cyt c is higher than the non-covalently immobilized Cyt *c*. The surface concentrations and electrocatalytic activity of non-covalent immobilized Cyt *c* was found to be higher than the covalently immobilized Cyt c on SAM of 4-ATP. The rate constants and electrocatalytic activity of Cyt c-SWNT is significantly higher than the covalent and non-covalently immobilized Cyt *c* on 4-ATP. The electrocatalytic activities of Myb, and HRP are higher than the Cyt *c* modified electrodes. All the modified surfaces have been characterized using AFM and STM to understand the surface distribution of the immobilized species.

5.5 References

[1] F. A. Armstrong, G. S. Wilson. *Electrochim. Acta.* **2000**, *45*, 2623.

[2] A. Ulman, *Chem. Rev.* **1996**, *96*, 1533.

[3] Y. Wu, J. S. Hudson, Q. Lu, J. M. Moore, A. S. Mount, A. M. Rao, E. Alexov, P. C. Ke, *J. Phys. Chem. B* **2006**, *110*, 2475.

[4] F. A. Armstrong, H. A. O. Hill, N. J. Walton, *Acc. Chem. Res*. **1988**, *21*, 407.

[5] S. Song, R. A. Clark, E. F. Bowden, *J. Phys. Chem.* **1993**, *97*, 6564.

[6] R. A. Clark, E. F. Bowden, *Langmuir* **1997**, *13*, 559.

[7] T. M. Nahir, E. F. Bowden, *Langmuir* **2002**, *18*, 5283.

[8] H. Liu, H. Yamamoto, J. Wei, D. H. Waldeck, *Langmuir* **2003**, *19*, 2378.

[9] F. N. Buchi, A. M. Bond, *J. Electroanal. Chem.* **1991**, *314*, 191.

[10] M. Morimoto, H. Tanaka, T. Kawai, *Surf. Sci*. **2005**, *580*, L103.

[11] P. Pandey, S. P. Singh, S. K. Arya, V. Gupta, M. Datta, S. Singh, B. D. Malhotra, *Langmuir* **2007**, *23*, 3333.

[12] W. Zheng, Y. F. Zheng, *Electrochem. Comm*. **2007**, *9*, 1619.

[13] P. M. Ajayan, *Chem. Rev*. **1999**, *99*, 1787.

[14] M. Hughes, M. S. P. Shaffer, A. C. Renouf, C. Singh, G. Z. Chen, D. J. Fray, A. H. Windle, *Adv. Mater*. **2002**, *14*, 382.

[15] J. W. G. Wildoer, L. C. Venema, A. G. Rinzler, R. E. Smalley, C. Dekker, *Nature* **1998**, *39*, 59.

[16] T. W. Odom, J. L. Huang, P. Kim, C. M. Lieber, *Nature* **1998**, *39*, 62.

[17] P. J. Britto, K. S. V. Santhanam P. M. Ajayan, *Bioelectrochem.Bioenerg.* **1996**, *41*, 121.

[18] S. S. Karajanagi, A. A. Vertegel, R. S. Kane, J. S. Dordick, *Langmuir* **2004**, *20*, 11594.

[19] J. J. Gooding, R. Wibowo, J. Liu, W. Yang, D. Losic, S. Orbons, F. J. Mearns, J. G. Shapter, D. B. Hibbert, *J. Am. Chem. Soc.* **2003**, *125*, 9006.

[20] B. R. Azamian, J. J. Davis, K. S. Coleman, C. B. Bagshaw, M. L. H. Green, *J. Am. Chem. Soc*. **2002**, *124*, 12664.

[21] J. Wang, M. Musameh, Y. Lin, *J. Am. Chem. Soc*. **2003**, *125*, 2408.

[22] R. Bandyopadhyaya, E. N. Roth, O. Regev, R. Y. Rozen, *Nano. Lett*. **2002**, *2*, 25.

[23] J. Tkac, T. Ruzgas, *Electrochem. Comm*. **2006**, *8*, 899.

[24] R. A. Clark, E. F. Bowden, *Langmuir* **1997**, *13*, 559.

[25] S. Song, R. A. Clark, E. F. Bowden, *J. Phys. Chem*. **1993**, *97*, 6564.

[26] S. I. Imabayashi, T. Mita, Z. Q. Feng, M. Iida, K. Niki, T. Kakiuchi, *Electrochemistry* **1997**, *65*, 467.

[27] V. Batz, M. A. Schneeweiss, D. Kramer, H. Hagenström, D. M. Kolb, D. Mandler, *J. Electroanal. Chem.* **2000**, *491*, 55.

[28] V. Ganesh, R. R. Pandey, B. D. Malhotra, V. Lakshminarayanan, *J. Electroanal. Chem.* **2008**, *619*, 87.

[29] N. Y. Suk, J. W. Choide. *J. Microbiol. Biotechnol*. **2006**, *16*, 15.

[30] S. Si, L, Si. F. Ren, D. Zhu, Y. Fung, *J. Coll. Inetrf. Sci.* **2002**, *253*, 47.

[31] S.-J. Xiao, M. Wieland, S. Brunner, *J. Coll. Interf. Sci.* **2005**, *290*, 172.

[32] M. Pita, S. Shleev, T. Ruzgas, V. M. Fernández, A. I. Yaropolov, L. Gorton, *Electro. Comm.* **2006**, *8*, 747.

[33] J. Wei, H. Liu, A. R. Dick, H. Yamamoto, Y. He, D. H. Waldeck, *J. Am. Chem. Soc.* **2002**, *124*, 9591.

[34] S. i. Imabayashi, T. Mita, T. Kakiuchi, *Langmuir* **2005**, *21*, 1470.

[35] J. J. Davis, C. M. Halliwell, H. A. O. Hill, G. W. Canters, M. C. V. Amsterdam, M. P. Verbeet, *New J. Chem*. **1998**, *22*, 1119.

[36] S. Mohanapriya, V. Lakshminarayanan, *Talanta* **2007**, *71*, 493.

[37] R. Bandyopadhyaya, E. Nativ-Roth, O. Regev, R. Yerushalmi-Rozen, *Nano Lett*. **2002**, *2*, 25.

[38] J. Wang, M. Musameh, Y. Lin, *J. Am. Chem. Soc*. **2003**, *125*, 2408.

[39] W. Zheng, Q. Li, Y. Yan, L. Su, L. Mao, *Indian J. Chem*. **2005**, *43A*, 950.

[40] R. Zhang, X. Wang, K.K. Shiu, *J. Colloid and Int. Sci.* **2007**, *316*, 517.

[41] M. C. Kum, K. A. Joshi, W. Chen, N. V. Myung, A. Mulchandini, *Talanta* **2007**, *74*, 370.

[42] H.A. Harbury, P. A. Loach, *J. Biol. Chem*. **1960**, *235*, 3640.

[43] A. L. Raphael, H. B. Gray, *J. Am. Chem. Soc*. **1991**, *113*, 1038.

[44] R. A. Clark, E. F. Bowden, *Langmuir* **1997**, *13*, 559.

[45] Z. Dai, S. Liu, H. Ju, *Electrochim. Acta* **2004**, *49*, 2139.

[46] S. Iijima, *Nature* **1991**, *354*, 56.

[47] J. Liu, A. Chou, W. Rahmat, M. N. Paddon-Row, J. J. Gooding, *Electroanalysis* **2005**, *17*, 38.

[48] Y. Yan, W. Zheng, M. Zhang, L. Wang, L. Su, L. Mao, *Langmuir* **2005**, *21*, 6560.

[49] B. Munge, G. Liu, G. Collins, J. Wang, *Anal. Chem*. **2005**, *77*, 4662.

[50] L. Chen, G. Lu, *J. Electroanal. Chem*. **2006**, *597*, 51.

[51] K. B. Gobi, F. Mizutani, *J. Electroanal. Chem*. **2000**, *484*, 172.

[52] G. C. Zhao, Z. Z. Yin, L. Zhang, X. W. Wei, *Electrochem. Comm*. **2005**, *7*, 256.

[53] H. Ju, S. Liu, B. Ge, F. Lisdat, F. W. Scheller, *Electroanalysis* **2002**, *14*, 141.

[54] G. C. Zhao, Z. Z. Yin, L. Zhang, X. W. Wei, *Electrochem. Comm*. **2005**, *7*, 256.

[55] H. Ju, S. Liu, B. Ge, F. Lisdat, F. W. Scheller, *Electroanalysis* **2002**, *14*, 141.

[56] J. J. Feng, G. Zhao, J. J. Xu, H. Y. Chen, *Anal. Biochem*. **2005**, *342*, 280.

[57] J. J. Gooding, R. Wibowo, J. Liu, W. Yang, D. Losic, S. Orbons, F. J. Mearns, J. G. Shapter, D. B. Hibbert, *J. Am. Chem. Soc*. **2003**, *125*, 9006.

[58] F. Patolsky, Y. Weizmann, I. Willner, *Angew. Chem. Int. Ed*. **2004**, *43*, 2113.

[59] X. Yu, B. Munge, V. Patel, G. Jensen, A. Bhirde, J. D. Gong, S. N. Kim, J. Gillespie, J. S. Gutkind, F. Papadimitrakopoulos, J. F. Rusling, *J. Am. Chem. Soc*. **2006**, *128*, 11199.

[60] B. R. Azamian, J. J. Davis, K. S. Coleman, C. B. Bagshaw, M. L. H. Green**,** *J. Am. Chem. Soc*. **2002**, *124*, 12664.

[61] N. W. S. Kam, H. Dai, *J. Am. Chem. Soc.* **2005**, *127*, 6021.

[62] C. Richard, F. F. Balavoine, P. Schultz, T. W. Ebbesen, C. Mioskowski, *Science* **2003**, *300*, 775.

[63] E. Katz, I. Willner, Chem.Phys.Chem. 5 (2004) 1084-1104.

[64] A. Bianco, M. Prato, *Adv. Mater.* **2003**, *15*, 1765.

[65] J. Wang, *Electroanalysis* **2005**, *17*, 7.

[66] H. A. Heering, K. A. Williams, Simon de Vries, C. Dekker, *Chem. Phys. Chem* **2006**, *7*, 1705.

[67] S. S. Karajanagi, A. A. Vertegel, R. S. Kane, J. S. Dordick, *Langmuir* **2004**, *20*, 11594.

[68] J. C. Kendrew, G. Bodo, H. M. Dintzis, R. G. Parrish, H. W. Wyckoff, D. C. Phillips, *Nature* **1958**, *181*, 622.

[69] E. Antonini, M. Brunori, *Hemoglobin and Myoglobin in their Reactions with Ligands. New York: American Elsevier Publishing Company,* **1971**.

[70] J. C. Kendrew, *Sci. Amer*. **1961,** *205*, 96.

[71] N. K. Boardman, S. M. Partridge *Biochem. J.* **1955**, *59*, 543.

[72] D. H. Spackman, W. H. Stein, S. Moore, *Anal. Chem*. **1958**, *30*, 1190.

[73] A. B. Edmundson, C. H. W. Hirs, *Nature*, **1961**, *190*, 663.

[74] T. Takano, *J. Mol. Biol*. **1977**, *110*, 537.

[75] A. B. Edmundson, *Nature* **1965**, *205*, 883.

[76] T. Hayashi, Y. Hitomi, T. Ando, T. Mizutani, Y. Hisaeda, S. Kitagawa, H. Ogoshi, *J. Am. Chem. Soc*. **1999**, *121*, 7747.

[77] L. Zhao, H. Liu, N. J. Hu, *J. Coll. Interf. Sci*. **2006**, *296*, 204.

[78] G. C. Zhao, L. Zhang, X. N. Wei, Anal. Biochem. **2004**, *329*, 160.

[79] J. Zhang, M. Oyama, *J. Electroanal. Chem*. **2005**, *577*, 273.

[80] H. M. Zhang, N. Q. Li, *Bioelectrochem*. **2000**, *53*, 97.

[81] S. Boussaad, N. J. J. Tao, *J. Am. Chem. Soc*. **1999**, *121*, 4510.

[82] F. Patolsky, Y. Weizmann, I. Willner, *Angew. Chem. Int. Ed*. **2004**, *43*, 2113.

[83] A. G. Elie, C. Lei, R. H. Baughman, *Nanotechnology* **2002**, *13*, 559.

[84] J. Wang, M. Li, Z. Shi, N. Li, Z. Gu, *Anal. Chem*. **2002**, *74*, 1993.

[85] J. Li, J. Yan, Q. Deng, G. Cheng, S. Dong, *Electrochim. Acta* **1997**, *42*, 961.

[86] S. Song, R. A. Clark, E. F. Bowden, M. J. Tarlov, *J. Phys. Chem*. **1993**, *97*, 6564.

[87] M. J. Tarlov, E. F. Bowden, *J. Am. Chem. Soc*. **1991**, *113*, 1847.

[88] M. Collinson, E. F. Bowden, M. J. Tarlov, *Langmuir* **1992**, *8*, 1247.

[89] E. Laviron, *J. Electroanal. Chem*. **1979**, *101*, 19.

[90] C. Phelps, L. Forlani, E. Antonini, *Biochem. J.* **1971**, *124*, 605.

[91] X.-f. Ding, G.-f. Yang, X. Wang, Z.-c. Wang, H.-b. Lin, *J. Electroanal. Chem*. **1983**, *151*, 311.

[92] L. Gorton, G. Jönsson-Pettersson, E. Csöregi, K. Johansson, E. Domínguez G. Marko-Varga *Analyst* **1992**, *117*, 1235.

[93] T. Lötzbeyer, W. Schuhmann, H.-L. Schmidt *Bioelectrochem. Bioenerg*. **1997**, *42*, 1.

[94] J. Li, S. Dong, *J. Electroanal. Chem*. **1997**, *431*, 19.

[95] Y.-D. Zhao, W.-D. Zhang, H. Chen, Q.-M. Luo, S. F. Y. Li, *Sens. Actuat. B* **2002**, *87*, 168.

[96] C. X. Cai, J. Chen, *Acta Chimi. Sini.* **2004**, *62*, 335.

[97] C. Cai, J. Chen, *Anal. Biochem.* **2004**, *325*, 285.

[98] F. Zhao, X. Wu, M. Wang, Y. Liu, L. Gao, S. Dong, A*nal. Chem.* **2004**, *76*, 4960.